8-30-2006

Oxygen isotope evidence for subduction and rift-related mantle metasomatism beneath the Colorado Plateau-Rio Grande rift transition

George Perkins

Zachary Sharp

Jane Selverstone

Contrib Mineral Petrol (2006) 151: 633–650
DOI 10.1007/s00410-006-0075-6

ORIGINAL PAPER

George B. Perkins · Zachary D. Sharp
Jane Selverstone

Oxygen isotope evidence for subduction and rift-related mantle metasomatism beneath the Colorado Plateau–Rio Grande rift transition

Received: 8 October 2005 / Accepted: 14 February 2006 / Published online: 15 March 2006

Abstract Spinel lherzolite and pyroxenite xenoliths from the Rio Puerco Volcanic Field, New Mexico, were analyzed for oxygen isotope ratios by laser fluorination. In lherzolites, olivine $\delta^{18}O$ values are high (+5.5‰), whereas $\delta^{18}O$ values for pyroxenes are low (cpx = +5.1‰; opx = +5.4‰) compared to average mantle values. Pyroxenite $\delta^{18}O$ values (cpx = +5.0‰; opx = +5.3‰) are similar to those of the lherzolites and are also lower than typical mantle oxygen isotope compositions. Texturally and chemically primary calcite in pyroxenite xenoliths is far from isotopic equilibrium with other phases, with $\delta^{18}O$ values of +21‰. The isotopic characteristics of the pyroxenite xenoliths are consistent with a petrogenetic origin from mixing of lherzolitic mantle with slab-derived silicate and carbonatite melts. The anomalously low $\delta^{18}O$ in the pyroxenes reflects metasomatism by a silicate melt from subducted altered oceanic crust, and high $\delta^{18}O$ calcite is interpreted to have crystallized from a high $\delta^{18}O$ carbonatitic melt derived from subducted ophicarbonate. Similar isotopic signatures of metasomatism are seen throughout the Rio Puerco xenolith suite and at Kilbourne Hole in the southern Rio Grande rift. The discrete metasomatic components likely originated from the subducted Farallon slab but were not mobilized until heating associated with Rio Grande rifting occurred. Oxygen diffusion modeling requires that metasomatism leading to the isotopic disequilibrium between calcite and pyroxene in the pyroxenites occurred immediately prior to entrainment. Melt infiltration into spinel-facies mantle (xenoliths) prior to eruption was thus likely connected to garnet-facies melting that resulted in eruption of the host alkali basalt.

Communicated by J. Hoefs

G. B. Perkins · Z. D. Sharp (✉) · J. Selverstone
Department of Earth and Planetary Sciences,
University of New Mexico, MSC03 2040,
Albuquerque, NM 87131-0001, USA
E-mail: zsharp@unm.edu
Tel.: +1-505-2772000
Fax: +1-505-2778843

Introduction

The Rio Puerco Volcanic Field (RPVF) in New Mexico straddles the boundary between the Colorado Plateau to the west and the Rio Grande rift to the east (Fig. 1a). Pliocene alkali basalts from the Rio Puerco field bring abundant mantle xenoliths to the surface, providing samples of the subcontinental mantle lithosphere in a region that has been profoundly modified by Tertiary tectonism. Although the surface expressions of the Laramide orogeny and Rio Grande rifting are obvious, the effects of these events on the composition of the mantle lithosphere are not well known. Xenoliths from the Colorado Plateau and from a few localities within the Rio Grande rift have been studied in detail (see Wilshire et al. 1988 for an overview), but the RPVF has been largely overlooked despite its transitional tectonic setting.

Although most mantle peridotite xenoliths show a narrow range in oxygen isotope compositions (Mattey et al. 1994), some localities display variations from typical mantle values. Subduction-related processes have been called upon to explain unusual oxygen isotope compositions in mantle-derived basalts and xenoliths from many geologic settings, including those not associated with active subduction zones such as ocean island hot spots and mid-ocean ridges (Eiler et al. 1997, 1998, 2000; Lassiter and Hauri 1998; Cooper et al. 2004; Xia et al. 2004; Macpherson et al. 2005). Eclogite xenoliths, which are generally interpreted as remnant oceanic crust, have been found to retain both high and low oxygen isotope compositions in the mantle for over 1 B.y. following subduction (MacGregor and Manton 1986; Ongley et al. 1987; Eiler 2001). Oxygen isotope geochemistry thus provides a means of identifying melt or fluid derived from subducted oceanic crust.

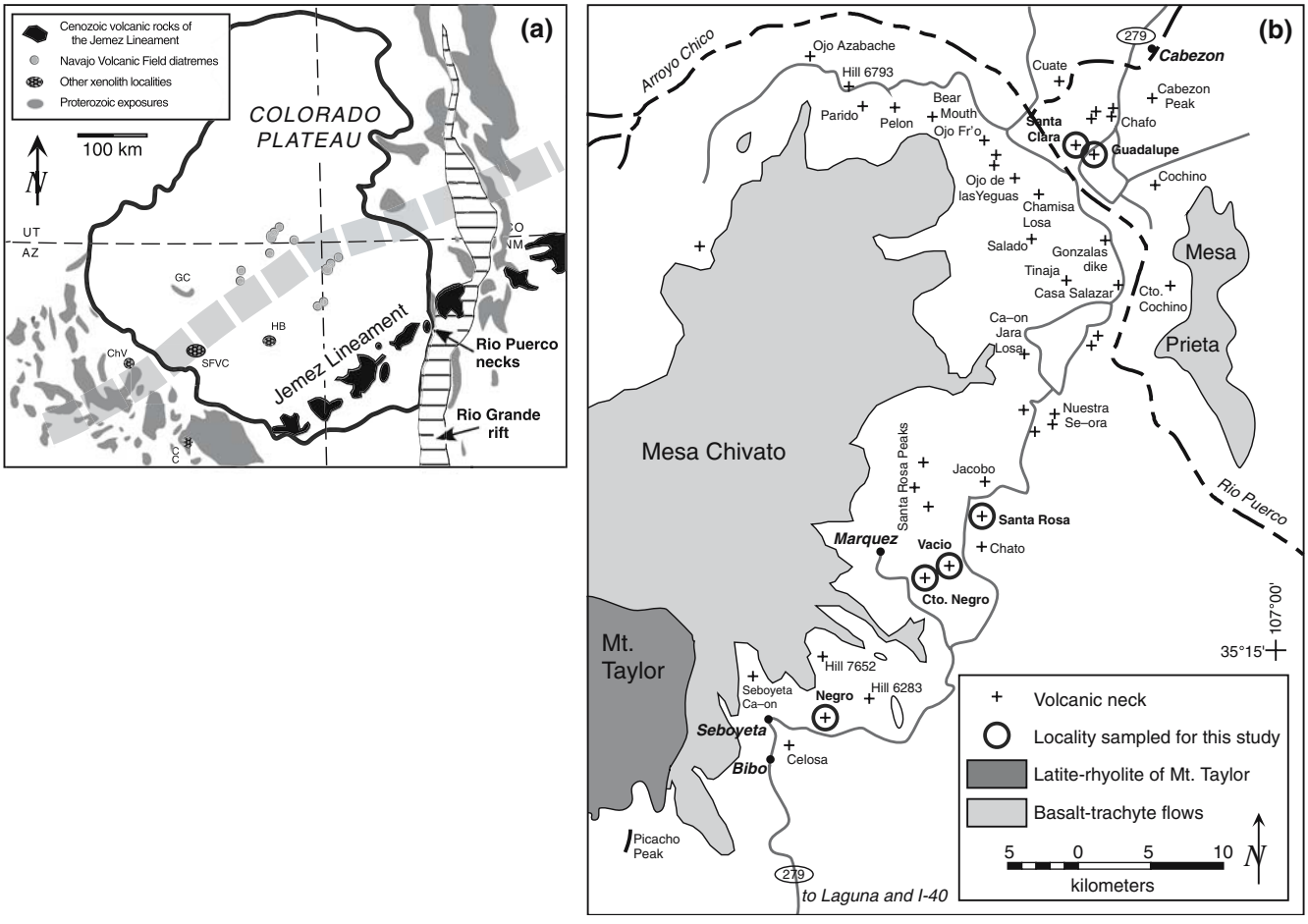

Fig. 1 **a** Map showing location of the Rio Puerco volcanic necks at the intersection between the Colorado Plateau, the Rio Grande rift, and the Jemez Lineament. **b** Map showing location of individual necks within the Rio Puerco field. After Hallett et al. (1997)

This study presents oxygen isotope compositions of mineral separates from 34 pyroxenite and spinel lherzolite xenoliths from 6 volcanic necks in the RPVF. The xenolith suite from the RPVF is unusual among xenolith localities in that it includes a wide range of modal compositions, an unusually high proportion of pyroxenite xenoliths, a range of metasomatic and oxidation features, and many xenoliths that contain carbonate as a primary phase. Using oxygen isotope geochemistry of the RPVF xenoliths, this study seeks to link textural observations with oxygen isotope variations to constrain the timing and source of the metasomatic agents at the Rio Grande Rift–Colorado Plateau transition. These results are compared to other oxygen isotope data from mantle xenoliths from Kilbourne Hole (this study), in the southern Rio Grande rift (Kyser et al. 1981), and the Colorado Plateau (The Thumb: Mattey et al. 1994). The petrogenesis of pyroxenites in the mantle remains poorly understood, and oxygen isotope geochemistry in conjunction with petrologic constraints may elucidate possible origins. This study contains the largest number of mantle xenolith samples from a single locality ever analyzed for oxygen isotope composition, thereby providing an opportunity to examine the heterogeneity among oxygen isotopes in the mantle over a small scale.

Tectonic history and geologic setting

The RPVF is located in central New Mexico, between the Colorado Plateau and the Rio Grande Rift (Fig. 1a). This region has experienced several tectonic events following accretion to North America at 1.6–1.7 Ga (Condie 1986). The latest tectonic event occurred in the last 30 M.y. with extension and opening of the Rio Grande Rift, a series of north–south trending grabens reaching from the Colorado–Wyoming border to northern Mexico (Keller et al. 1991). Both the crust and lithosphere are unusually thin beneath the Rio Grande Rift (30–40 km, 45–55 km, respectively), based on recent seismic transects (Gao et al. 2004; West et al. 2004; Wilson et al. 2005a, b). At a depth of 100 km, seismic velocities beneath the Rio Grande Rift are ~3–4% slower than the adjacent Colorado Plateau and Great Plains (Gao et al. 2004), suggesting a large temperature or compositional contrast, and/or the presence of partial

melt beneath the rift. However, the 410 and 660 km discontinuities are not deflected beneath the rift, indicating the thermal and/or compositional anomaly is a feature of only the uppermost mantle (Wilson et al. 2005a). Rift-related volcanism shows a temporal shift in ε_{Nd} from low (−8 to +2) to high (+4 to +8) values, reflecting a change from enriched to depleted mantle source regions (McMillan 1998). This shift in source regions may indicate a transition from a lithospheric mantle to asthenospheric source for melt generation (Perry et al. 1987, 1988). Together, the seismic data and radiogenic isotope data suggest crustal and lithospheric thinning, asthenospheric upwelling, and high temperatures and/or partial melt beneath the Rio Grande Rift.

To the west of the RPVF, the Colorado Plateau is characterized by high elevations and minimal tectonic activity since the Cretaceous, although the Colorado Plateau may have rotated en masse as a semi-stable microplate during this interval (Cather 1999; Wawrzyniec et al. 2002). Seismic profiles across the Colorado Plateau suggest unusually thick crust (42–55 km) and lithosphere (120–150 km or more) (Gao et al. 2004; West et al. 2004). A cold and depleted mantle root has been proposed to account for the tectonic stability of the Colorado Plateau (Smith 2000; Lee et al. 2001). Although present in the Four Corners region, Tertiary volcanism is uncommon in the Colorado Plateau and is largely limited to its periphery. The southeastern margin of the Colorado Plateau coincides with the Jemez lineament, a series of Tertiary volcanic centers trending NE–SW characterized by high heat flow and low seismic velocities (Aldrich and Laughlin 1984). Although the nature of the Jemez lineament is enigmatic, it parallels the regional Precambrian fabric, leading to speculation that preexisting structural weaknesses facilitated volcanism (Karlstrom and Humphreys 1998; Shaw et al. 1998).

The most recent subduction event in southwestern North America is associated with the Laramide orogeny in the late Cretaceous and early Tertiary. Although the RPVF is located over 1,500 km from the continental margin, it is generally accepted that low-angle subduction of a young and buoyant Farallon oceanic plate induced orogenesis well within the continental interior (Atwater 1970; Coney and Reynolds 1977; Bird 1988). It is generally thought that the oceanic slab was located directly beneath the subcontinental mantle lithosphere, displacing the overlying asthenospheric mantle wedge and maintaining relatively cold temperatures in the overlying lithosphere (Dumitru et al. 1991; Smith 1995; Riter and Smith 1996; Humphreys et al. 2003). Seismic imaging suggests a foundering slab currently at depths of ~600 km (Van der Lee and Nolet 1997; Bunge and Grand 2000). The removal of the slab from the base of the lithosphere and resultant influx of asthenosphere may be associated with the high topography of the Colorado Plateau and extension of the Rio Grande Rift (Humphreys et al. 2003).

The pyroxenite and lherzolite xenoliths of this study occur in Pliocene alkali basalt volcanic necks in the RPVF (Fig. 1b), dated at 4.49–2.05 Ma (Hallett et al. 1997). The petrology and geochemistry of the host basalts are detailed in Hallett (1994). Normal faults in the RPVF region are associated with extension at the western margin of the Rio Grande Rift; these both predate and locally postdate volcanism, indicating ongoing rifting (Hallett et al. 1997). Mantle xenoliths are present in approximately half of the ~50 volcanic necks in the RPVF (Hallett 1994). Crustal xenoliths and spinel and clinopyroxene megacrysts also occur in the RPVF suite. The mantle xenoliths for this study were collected from six of the volcanic necks: Cerro Negro, Cerrito Negro, Cerro Vacio, Cerro de Santa Rosa, Cerro de Guadalupe, and Cerro de Santa Clara. These volcanic necks span a 100 km distance through the volcanic field, thereby providing the opportunity to obtain a transect across the mantle in this region.

Spinel lherzolite xenoliths from Kilbourne Hole, in the Potrillo volcanic field in southern New Mexico, were also analyzed in this study. The Potrillo volcanic field is located within the axis of the southern Rio Grande Rift, and is dated at 80,000 years (Bussod and Williams 1991). High ε_{Nd} values of +4.7 to +6.3 suggest an asthenospheric source for the host basanites (McMillan et al. 2000). Pyroxenite and crustal xenoliths, and clino- and orthopyroxene megacrysts are also present at Kilbourne Hole (Padovani and Reid 1989).

Sample description

The xenoliths studied are spinel lherzolites, spinel pyroxenites, and spinel-free pyroxenites. These were selected from a larger collection of xenoliths for their larger grain size, lack of alteration, minimal evidence for interaction with host basalt, and to provide a suite that allowed for comparison of different xenolith textures and samples from different volcanic necks.

Lherzolite samples contain ~50% olivine, ~30% clinopyroxene, ~15% orthopyroxene, and ~5% spinel; however, proportions vary somewhat, and some "lherzolite" samples have less than 40% olivine, placing them within the olivine websterite field. For this study, we classify any xenolith with more than ~10% olivine as a lherzolite, and those with little to no olivine are classified as pyroxenites.

Lherzolite samples from the RPVF exhibit a granular to protogranular texture, with grains of orthopyroxene and/or olivine up to 2 mm in diameter surrounded by smaller grains (Fig. 2a). In lherzolites, spinels are brown in color, reflecting high Mg and Cr contents, and are small, irregularly-shaped grains located along grain boundaries. In some cases, a reaction product of glass ± plagioclase ± olivine surrounds spinel grains, which is interpreted as a decompression feature formed during ascent. Deformation bands and subgrain boundaries are common in olivine and locally present in pyroxenes, but deformation features are not ubiquitous in the RPVF xenoliths. In lherzolites from the northern

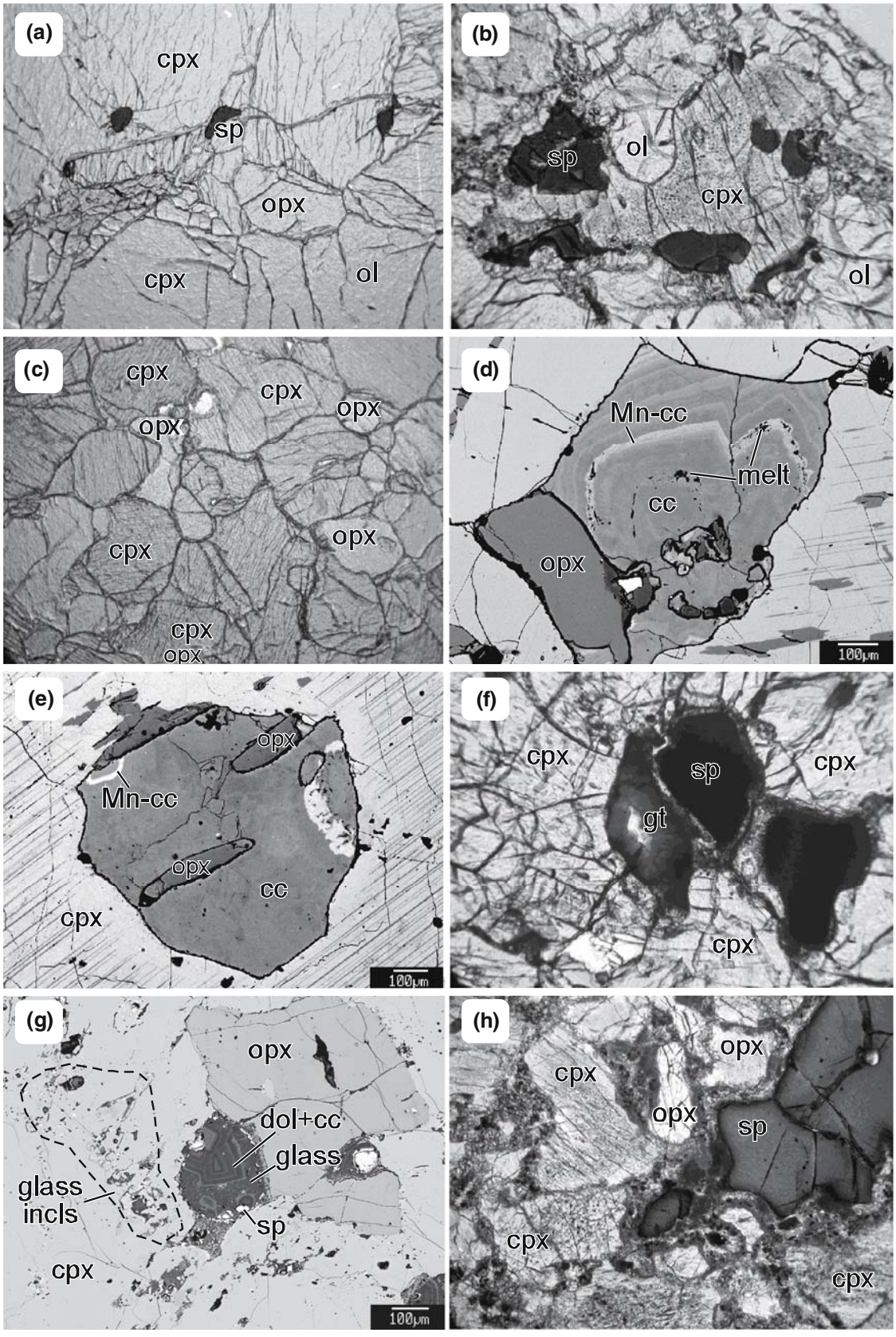

volcanic necks (Cerro de Guadalupe and Cerro de Santa Clara), a subtle foliation is indicated by a shape-preferred pyroxene orientation and planar concentrations of spinel. Deformation microfabrics are less commonly observed in the xenoliths from the southern volcanic necks. Two of the studied lherzolites (CSR27

◄

Fig. 2 Photomicrographs and back-scattered electron (BSE) images of representative xenolith features. **a** Typical unaltered spinel lherzolite (CG38). FOV = 4 mm. **b** Spinel lherzolite (CN4) with spongy clinopyroxene. Fluid/melt inclusions occur only in clinopyroxene. FOV = 4 mm. **c** Spinel-absent pyroxenite (CTON1). FOV = 4 mm. **d** BSE image of calcite in spinel-absent pyroxenite (CTON7). Note Mn-rich growth bands and zones with melt inclusions. **e** BSE image of calcite inclusion in clinopyroxene in CTON7, showing inclusions of orthopyroxene in calcite. **f** Black spinel-bearing pyroxenite (CTON6). Note relic garnet with glass/keliphyte rim. FOV = 2 mm. **g** BSE image of calcite + dolomite globule associated with spinel and glass inclusions in black-spinel pyroxenite (CG40). **h** Green spinel-bearing pyroxenite (CV9). Note reaction rims around spinel and spongy clinopyroxene. FOV = 4 mm

and CTON57) show exsolution between clino- and orthopyroxene. Two lherzolites studied from Cerro de Santa Rosa (CSR20, CSR27) contain both green olivine and red altered olivine. Petrographically, the red color is a result of hair-like fibers; these are magnetite ± hematite based on TEM and rock magnetic analyses (Callahan et al. 2004). Carbonate is rare in lherzolite xenoliths, although sample CTON53 contains fine-grained carbonate associated with a reaction of spinel to melt. Authigenic carbonate, chlorite, and clay minerals also occur as alteration products in fractures in some lherzolite xenoliths.

Fluid and glass inclusions in lherzolite xenoliths are typically found along planar trains in clino- and orthopyroxene that locally continue across grain boundaries; however, some samples lack fluid inclusions altogether. Lherzolite xenoliths studied here (CSR27, CSR3, CN4) locally include spongy-textured clinopyroxene, and, less commonly, orthopyroxene (Fig. 2b). Glass is present along grain boundaries and within some clinopyroxene grains from Cerrito Negro lherzolites (CTON53, CTON57), but is nearly absent from the other studied lherzolites.

Pyroxenite xenoliths, characterized by a near absence of olivine, fall within three categories based on spinel characteristics. Mineral compositions for the different pyroxenite types are given in Porreca (2005, in preparation). Spinel-absent pyroxenites (SAPs) are found only at Cerrito Negro (CTON1, 2, 7, 10, 16, 55, 58) (Fig. 2c). The SAPs contain large clinopyroxene (< 3 mm in diameter) associated with smaller grains of orthopyroxene. Large augite grains typically exhibit exsolution between orthopyroxene and clinopyroxene, and also contain many small rounded inclusions of orthopyroxene. No prevalent foliation or deformation bands are seen in pyroxenes within the SAPs. Calcite is present in all but one (CTON16) of the SAPs studied, occurring as large discrete grains that exhibit thin growth bands defined by Mn-rich calcite and silicate glass inclusions (Fig. 2d). These discrete calcite grains are typically included within large clinopyroxene grains and are intimately intergrown with small orthopyroxene grains (Fig. 2d, e). Calcite also occurs at grain triple junctions where it is associated with silicate glass. Based on textural characteristics and the association with glass, the calcite is inferred to be of mantle origin. Fluid and glass inclusions are abundant in the SAPs.

Black spinel-bearing pyroxenites (BSPs) are present in xenoliths from Cerrito Negro, Cerro de Guadalupe, and Cerro de Santa Rosa. These contain large black spinels up to 2 mm in diameter that are hercynitic (Fe-rich) in composition. In two samples (CTON6, CTON17), the black spinels are associated with reaction rims around relict garnets (Fig. 2f), interpreted to have formed during decompression and heating prior to entrainment (Porreca 2005). Black spinel is typically rimmed by bands up to 0.2 mm wide of melt and recrystallized green spinels, or by wider reaction rims containing abundant plagioclase. Four of the BSPs (CTON9, CTON35, CG31, CG40) contain carbonate (calcite ± dolomite) associated with silicate glass and small green or black spinel grains (Fig. 2g). This assemblage is interpreted as quenched melt that formed in situ. Phlogopite is present in one BSP studied (CTON35), suggesting local mantle hydration. Melt occurs as glass inclusions in many of the pyroxenes and along grain boundaries in most of the Cerrito Negro BSPs, although it is not observed in the Cerro de Guadalupe or Cerro de Santa Rosa samples. Large pyroxene grains, up to 3 mm in diameter, are surrounded by smaller pyroxenes in many of the BSPs. Coarse exsolution between clino- and orthopyroxene is seen in the BSPs from Cerrito Negro; these samples also have rounded orthopyroxene inclusions in clinopyroxene, much like the Cerrito Negro SAPs. BSPs from other volcanic necks show little to no exsolution in the pyroxenes. Glass inclusions are present along planar inclusion trains in nearly all of the BSPs, although spongy textured clinopyroxene is present in only one sample studied for isotopic analysis (CSR4). No foliation or deformation textures are seen in the BSPs.

Green spinel-bearing pyroxenites (GSPs) are present in xenoliths from Cerro Vacio, Cerro de Santa Rosa, and Cerrito Negro. These are distinguished from the BSPs by the presence of large (0.5–4 mm in diameter) green spinel with darker rims; this zoning may reflect Mg-rich cores with Fe-rich rims (Fig. 2h). In the GSPs, spinels are always associated with reaction rims rich in glass and plagioclase. Although most GSPs have a granoblastic texture, others contain large clinopyroxene megacrysts. Spongy clinopyroxenes with abundant fluid/melt inclusions are common in the GSPs, and fluid inclusions also locally occur in planar trains in orthopyroxene. Glass is present in many fractures and grain boundaries in the GSPs from Cerrito Negro and Cerro de Santa Rosa. In the Cerro Vacio GSPs, glass is present in large reaction zones of fine-grained brown alteration with plagioclase, olivine, clinopyroxene, and small Fe-rich spinel grains. No deformation textures or prevalent foliation occur in the GSPs, with the exception of CTON56, which shows undulatory extinction in ortho- and clinopyroxene, indicating subgrain development.

A pyroxenite from Cerro de Santa Clara (CSC25), containing small brown spinels similar to the spinel in the lherzolites, was analyzed for oxygen isotope composition. This sample has a granoblastic texture with no obvious deformation microstructures. Fluid inclusions are present along planar trains in clinopyroxene and orthopyroxene.

The Kilbourne Hole spinel lherzolite xenoliths are medium to coarse-grained and have a protogranular texture with no prevalent fabric. These xenoliths were not examined in thin section, but are probably equivalent to the Group I protogranular lherzolites described by Roden et al. (1988), and Kil and Wendlandt (2004). Petrographic descriptions, bulk rock geochemistry and mineral compositions from similar xenoliths from Kilbourne Hole are well documented (Kyser et al. 1981; Roden et al. 1988; Kil and Wendlandt 2004).

Methods

Mineral separates from 38 xenoliths were analyzed for their oxygen isotope composition. For preparation, the surrounding basalt and alteration rinds were cut and removed. Samples were crushed, sieved to 30–60 mesh, cleaned in an ultrasonic bath for 30 min, and dried at 50°C for a minimum of 24 h. Approximately 15–20 grains of each mineral present (olivine, clinopyroxene, orthopyroxene, spinel, and calcite) were handpicked under a dissecting microscope. Mineral grains were preferentially chosen to avoid grains with discernable mineral inclusions or alteration. For each mineral, 1.5–2.5 mg of the separates were placed in a laser extraction line under vacuum for 48 h prior to fluorination and oxygen isotope analysis.

Oxygen isotope analyses for silicates and spinel were made using the laser fluorination method of Sharp (1990). Samples were heated with a 25-W Merchantek CO_2 laser in a BrF_5 or F_2 atmosphere, releasing O_2. Unreacted reagent and SiF_4 produced by fluorination were frozen in a liquid nitrogen U-trap and excess F_2 was neutralized with a heated NaCl trap. Purified O_2 was collected in a zeolite cold finger prior to introduction into the mass spectrometer. $\delta^{18}O$ values were measured on a Finnigan MAT Delta XL mass spectrometer at the Stable Isotope Laboratory at the University of New Mexico. Garnet standard UWG-2 ($\delta^{18}O = +5.8‰$, Valley et al. 1995) and an in-house quartz standard Lausanne-1 ($\delta^{18}O = +18.2‰$) were analyzed during each run to ensure accuracy. Twenty-seven UWG-2 analyses yielded $\delta^{18}O = +5.76 \pm 0.16‰$ (1.s.d.); thus, values are accurate to better than 0.2‰. All data are reported in the standard $\delta^{18}O$ notation relative to SMOW, where $\delta^{18}O_{NBS\text{-}28} = +9.65‰$ relative to SMOW (Hut 1987).

Calcite separates of 1.5–2.5 mg from four samples (CTON1, 2, 7 and CG40) were analyzed for oxygen and carbon isotopes. CO_2 was extracted from calcite at 50°C with phosphoric acid (McCrea 1950). Aliquots of CO_2 were sampled automatically and introduced to the mass spectrometer in a continuous He flow. An in-house reference standard of Carrara marble calcite ($\delta^{18}O = +29.31‰$, $\delta^{13}C = +1.96‰$) was used to assess the accuracy of the mass spectrometer. Oxygen isotopes of calcite are reported in $\delta^{18}O$ notation relative to SMOW, and carbon isotopes are reported in $\delta^{13}C$ notation relative to PDB, where $\delta^{18}O_{NBS\text{-}19} = -2.2‰$ relative to SMOW and $\delta^{13}C_{NBS\text{-}19} = +1.95‰$ relative to PDB. Carbonate samples were run in duplicate and averaged.

Results

Oxygen isotope compositions for silicate minerals from 18 spinel lherzolites and 20 pyroxenites and $\delta^{13}C$ and $\delta^{18}O$ values for calcite from 4 pyroxenites are shown in Tables 1 and 2 and plotted in Figs. 3, 4, 5. The fractionations between coexisting mineral phases ($\Delta^{18}O_{x-y}$) are also noted, where $\Delta^{18}O_{x-y} = \delta^{18}O_x - \delta^{18}O_y$. For the RPVF lherzolites, mineral $\delta^{18}O$ values are as follows: olivine = +5.2 to +6.1‰ (avg. = +5.5‰, $1\sigma = 0.23‰$, $n = 14$), clinopyroxene = +4.8 to +5.5‰ (avg. = +5.1‰, $1\sigma = 0.28‰$, $n = 12$), orthopyroxene = +4.7 to +5.8‰ (avg. = +5.4‰, $1\sigma = 0.36‰$, $n = 13$), and spinel = +2.0 to +4.8‰ (avg. = +3.6‰, $1\sigma = 0.83‰$, $n = 11$). It should be noted that the RPVF lherzolites record negative $\Delta^{18}O_{cpx\text{-}ol}$ fractionations (Fig. 3b), which cannot be accounted for by closed system equilibrium between olivine and pyroxene. Variations in $\delta^{18}O$ do not readily correlate with textural evidence for metasomatism such as abundance of fluid inclusions or signs of melt presence. No systematic trends are seen between $\delta^{18}O$ value and location of the volcanic neck within the volcanic field, suggesting no major tectonic controls on the $\delta^{18}O$ values within the RPVF. $\delta^{18}O$ values of red olivines from two Cerro de Santa Rosa lherzolites (CSR20, 27) are indistinguishable from green (unoxidized) olivine from the same xenoliths, where all values for this sample fall toward the middle of the range of olivine $\delta^{18}O$ values from the RPVF, indicating that the oxidizing fluid had not effect on oxygen isotope ratios.

Oxygen isotope compositions of the four Kilbourne Hole xenoliths show the following ranges: olivine = +5.3 to +5.4‰; clinopyroxene = +5.2 to +5.4‰; orthopyroxene = +5.6 to +5.8‰; spinel = +4.6 to +5.0‰ (Table 1, Figs. 3, 4). These data, obtained by laser fluorination, show notably less variability than the results for three Kilbourne Hole xenoliths by Kyser et al. (1981) using conventional extraction techniques. The results for olivine, orthopyroxene, and spinel fall within the range of results obtained by Kyser et al. (1981); however, the clinopyroxene $\delta^{18}O$ values obtained by our study are notably lower than those of Kyser et al. (1981), and three of the four analyses show isotopic disequilibrium between olivine and clinopyroxene.

Compared to a global compilation of mantle spinel lherzolite xenoliths ($n = 27$, Mattey et al. 1994), the

Table 1 Oxygen isotopic composition of mineral separates from lherzolites

Sample	$\delta^{18}O$ SMOW (‰)				$\Delta^{18}O_{a\text{-}b}$ (‰)						T (°C)[a]
	Ol (red)	Cpx	Opx	Sp	Cpx-Ol	Opx-Ol	Sp-Ol	Opx-Cpx	Sp-Cpx	Sp-Opx	
CN1	5.2	4.8	5.4		−0.4	0.2		0.6			
CN4	5.5		5.8	3.9		0.3	−1.7			−1.9	941
CTON53	5.5	5.4	5.5	2.4	−0.1	−0.1	−3.2	0.0	−3.0	−3.1	696
CTON57	5.5	5.3	4.7	3.6	−0.3	−0.9	−2.0	−0.6	−1.7	−1.1	884
CSR3	6.1	4.8		4.1	−1.3		−2.0		−0.7		879
CSR7	5.5	5.5	4.8		0.1	−0.6		−0.7			
CSR17	5.4	4.8	5.8	3.9	−0.6	0.4	−1.5	1.0	−0.9	−1.9	981
CSR20	5.7 (5.6)	4.9	5.6	4.1	−0.8	−0.1	−1.6	0.7	−0.8	−1.5	956
CSR27	5.6 (5.5)	5.3	5.6	3.8	−0.3	0.0	−1.8	0.3	−1.4	−1.8	923
CG12	5.5		5.3	2.0		−0.2	−3.5			−3.3	655
CG16	5.2	4.8	5.6	2.9	−0.4	0.4	−2.3	0.8	−1.9	−2.6	825
CG38	5.6	5.1	5.5	4.8	−0.5	−0.1	−0.8	0.4	−0.3	−0.7	1,164
CSC14	5.2	5.4	5.2		0.3	0.0		−0.2			
CSC16	5.4	5.3	5.0	4.2	−0.1	−0.4	−1.2	−0.3	−1.1	−0.8	1,048
CN avg.	5.4	4.8	5.6	3.9	−0.4	0.2	−1.7	0.6		−1.9	
CTON avg.	5.5	5.4	5.1	3.0	−0.2	−0.5	−2.6	−0.3	−2.4	−2.1	
CSR avg.	5.6	5.1	5.5	4.0	−0.6	−0.1	−1.7	0.3	−1.0	−1.7	
CG avg.	5.4	5.0	5.5	3.2	−0.4	0.0	−2.2	0.6	−0.1	−2.2	
CSC avg.	5.3	5.4	5.1	4.2	0.1	−0.2	−1.2	−0.3	−1.1	−0.8	
RPVF avg. lherzolite	5.5	5.1	5.4	3.6	−0.4	−0.1	−1.9	0.2	−1.3	−1.9	
KH1	5.4	5.4	5.6	4.6	−0.1	0.2	−0.8	0.3	−0.8	−1.0	1,164
KH2	5.3	5.3	5.6	5.0	0.0	0.3	−0.3	0.2	−0.3	−0.6	1,340
KH3	5.3	5.2	5.8	4.9	−0.1	0.5	−0.4	0.6	−0.3	−0.9	1,301
KH4	5.4	5.2	5.8	4.7	−0.2	0.4	−0.7	0.6	−0.5	−1.1	1,195
Kilbourne Hole avg.	5.4	5.3	5.7	4.8	−0.1	0.3	−0.6	0.4	−0.5	−0.9	
KH conv. avg.[b]	5.2	5.6	5.8	4.5	0.4	0.6		0.2	−0.9	−1.8	
Colorado Plateau[c]	5.3	5.5	5.6		0.2	0.3		0.1			
Global avg.[c]	5.1	5.5	5.7		0.4	0.6		0.2			

[a]Temperatures calculated using theoretical fractionation factor between spinel and olivine from Zheng (1991, 1993)
[b]Average $\delta^{18}O$ values of three spinel lherzolite xenoliths from Kilbourne Hole, using conventional oxygen isotope extraction techniques (Kyser et al. 1981)
[c]Average $\delta^{18}O$ values for 12 garnet lherzolite xenoliths from the Thumb (Colorado Plateau), and global average $\delta^{18}O$ for 27 spinel lherzolite xenoliths, using laser fluorination (Mattey et al. 1994)

RPVF xenoliths show a larger range in $\delta^{18}O$ for all minerals and typically have olivine $\delta^{18}O$ values higher than the global average (+5.5‰ vs. +5.1‰), and $\delta^{18}O$ values for clinopyroxene and orthopyroxene less than the global average (+5.1‰ vs. +5.5‰, +5.4‰ vs. +5.7‰, respectively; Fig. 3). Olivine in garnet lherzolite xenoliths from The Thumb, in the Colorado Plateau (avg. $\delta^{18}O = +5.3$‰, $n = 12$, Mattey et al. 1994) and spinel lherzolite xenoliths from Kilbourne Hole (avg. $\delta^{18}O = +5.4$‰) also have higher $\delta^{18}O$ values than the mantle average. Pyroxene $\delta^{18}O$ values for The Thumb are similar to those of the typical mantle (Fig. 3a–c). The Kilbourne Hole xenoliths have orthopyroxene $\delta^{18}O$ values similar to those of the typical mantle, whereas clinopyroxene shows lower $\delta^{18}O$ values and negative $\Delta^{18}O_{cpx\text{-}ol}$ as seen also in the RPVF. Spinels from the RPVF lherzolites have an average $\delta^{18}O$ (+3.6‰) lower than those from Kilbourne Hole (+4.8‰).

Pyroxenites from the RPVF have the following $\delta^{18}O$ ranges: clinopyroxene = +4.3 to +5.4‰ (avg. = +5.0‰, $1\sigma = 0.25$‰, $n = 20$), orthopyroxene = +4.2 to +5.9‰ (avg. = +5.3‰, $1\sigma = 0.38$‰, $n = 19$), and spinel = +3.8 to +5.6‰ (avg. = +4.7‰, $1\sigma = 0.44$‰, $n = 13$). Pyroxene $\delta^{18}O$ values are only ~0.1‰ lower in pyroxenites than in lherzolites (Figs. 3c, d), whereas spinel $\delta^{18}O$ values are notably higher in pyroxenites than in lherzolites from the RPVF (Fig. 4). The $\delta^{18}O$ values do not readily correlate with pyroxenite type; SAPs, BSPs, and GSPs have average clinopyroxene and orthopyroxene $\delta^{18}O$ values within 0.1‰ of one another (omitting one outlier, CTON55 opx). Lower spinel $\delta^{18}O$ values are found in pyroxenites having undergone more metasomatism (e.g., CV9 and CV12), as evidenced by spongy textured clinopyroxene. Oxygen isotope studies of pyroxenites are scarce, and no published work exists from Colorado Plateau or Rio Grande Rift settings for pyroxenite xenoliths. Pyroxenites from the Beni Bousera peridotite massif, Morocco have a range of $\delta^{18}O$ clinopyroxene values from +4.9 to +9.3‰ (Pearson et al. 1991); in contrast, all clinopyroxene from the RPVF pyroxenites has $\delta^{18}O$ values less than +5.5‰ and a more restricted range. However, it is unclear whether the RPVF pyroxenites were formed by an analogous process to the massif pyroxenites.

Calcite in three spinel-absent pyroxenites from Cerrito Negro have $\delta^{18}O$ values of +21.3 to +21.8‰ (avg. = +21.5‰) and $\delta^{13}C$ values of −6.2 to −7.4‰ (avg. = −6.9‰; Fig. 5). Calcite from a BSP from Cerro de Guadalupe (CG40) has a $\delta^{18}O$ value of +25.1‰ and a $\delta^{13}C$ value of −0.6‰. The Cerrito Negro $\delta^{13}C$ values

Table 2 Oxygen and carbon isotopic composition of mineral separates from pyroxenites

Sample	Type	$\delta^{18}O$ SMOW (‰)			$\delta^{13}C$ (‰)			$\Delta^{18}O_{a\text{-}b}$ (‰)			T (°C)[a]
		Cpx	Opx	Sp	Cc	Cc	Opx-Cpx	Sp-Cpx	Sp-Opx	Cc-Cpx	
CTON1	SAP	4.9	5.2		21.4	−7.4	0.3			16.4	
CTON2	SAP	5.0	5.1		21.3	−6.2	0.1			16.2	
CTON6	BSP	5.0	5.1	4.9			0.1	0.0	−0.1		1,566
CTON7	SAP	4.6	5.1		21.8	−7.3	0.5			17.2	
CTON9	BSP	5.3	5.6	4.6			0.2	−0.7	−1.0		1,268
CTON10	SAP	5.0	5.7				0.7				
CTON16	SAP	4.9	5.3				0.4				
CTON17	BSP	5.0		5.6				0.6			
CTON35	BSP	5.0	4.9	4.9			−0.1	−0.2	−0.1		1,586
CTON46	GSP	4.9	5.7	4.9			0.7	−0.1	−0.8		1,322
CTON55	SAP	5.1	4.2				−0.8				
CTON56	GSP	5.4	5.9	4.7			0.5	−0.7	−1.2		1,207
CTON58	SAP	4.9	5.3				0.4				
CSR4	BSP	4.8	5.8	3.8			1.0	−1.0	−2.0		1,027
CSR5B	GSP	5.2	5.2	4.9			0.0	−0.3	−0.3		1,483
CV9	GSP	4.7	5.2	4.4			0.4	−0.3	−0.7		1,347
CV12	GSP	4.3	5.2	4.1			1.0	−0.2	−1.2		1,221
CG31	BSP	5.1	5.4	4.8			0.4	−0.3	−0.6		1,375
CG40	BSP	5.2	5.3	4.7	25.1	−0.6	0.1	−0.5	−0.6	19.9	1,105
CSC25	BrSP	4.9	5.7	4.5			0.8	−0.5	−1.2		1,206
SAP avg.		4.9	5.1		21.5	−6.9	0.2				
BSP avg.		5.0	5.4	4.8	25.1	−0.6	0.3	−0.3	−0.7		
GSP avg.		4.9	5.4	4.6			0.5	−0.3	−0.8		
CTON avg.		5.0	5.3	4.9	21.5	−6.9	0.3	−0.2	−0.6		
CSR avg.		5.0	5.5	4.3			0.5	−0.7	−1.2		
CV avg.		4.5	5.2	4.3			0.7	−0.2	−0.9		
CG avg.		5.1	5.4	4.7	25.1	−0.6	0.2	−0.4	−0.6		
CSC avg.		4.9	5.7	4.5			0.8	−0.5	−1.2		
RPVF avg. pyroxenite	5.0	5.3	4.7	22.4	−5.4	0.4	−0.3	−0.8	17.4		

[a]Temperature calculated using theoretical fractionation factors for spinel and orthopyroxene from Zheng (1991, 1993)

lie within the typical mantle range of −5 to −8‰ reported for carbon in xenoliths and carbonatites, however, the $\delta^{18}O$ values are well outside the range for primary carbonatites (+6 to +9‰) (Javoy et al. 1986; Deines and Haggerty 2000). Expected $\Delta^{18}O_{cc\text{-}cpx}$ fractionations at mantle temperatures are ~ 2–4‰ (Chiba et al. 1989; Rosenbaum et al. 1994a), so calcite could not have been in isotopic equilibrium with adjacent pyroxenes in the mantle. Other recent studies have reported unusually high calcite $\delta^{18}O$ values (>14‰) and disequilibrium fractionations between calcite and pyroxenes ($\Delta^{18}O_{cc\text{-}cpx}$ >10‰) in peridotite xenoliths from the East African Rift (Lee et al. 2000), the Pannonian Basin in Hungary (Demény et al. 2004), the Big Creek pipe in the central Sierra Nevada (Ducea et al. 2005), and in clinopyroxene megacrysts in kimberlites from the Slave Craton (van Achterbergh et al. 2002).

Discussion

Isotopic disequilibrium and metasomatizing fluids

The oxygen isotope compositions of the RPVF xenolith suite indicate that isotopic disequilibrium existed within the mantle prior to entrainment of the xenoliths in the host basalts. This section explores possible causes for the disequilibrium. The RPVF lherzolites have unusually high olivine $\delta^{18}O$ values and abnormally low clino- and orthopyroxene $\delta^{18}O$ values, when compared to typical mantle averages (Fig. 3). These discrepancies can not be explained by a single process, and require separate events to explain the olivine and the pyroxene data.

In the RPVF xenoliths, olivine typically shows little textural evidence for metasomatism, and the high $\delta^{18}O$ values may be representative of the region prior to the metasomatic event affecting pyroxene. As the xenoliths from The Thumb and Kilbourne Hole also have olivine $\delta^{18}O$ values above the mantle average, we suggest that ^{18}O enrichment over 'typical' mantle may be a regional phenomenon. An ^{18}O-rich fluid released during low-angle subduction of the Farallon slab has been proposed to explain high $\delta^{18}O$ values in hydrous eclogite xenoliths from the Navajo volcanic field (Smith 1995; Smith et al. 2004).

The negative $\Delta^{18}O_{px\text{-}ol}$ fractionations in the RPVF lherzolites are not predicted by theoretical calculations (Zheng 1993) nor supported by experimental studies (Chiba et al. 1989; Rosenbaum et al. 1994a). Negative $\Delta^{18}O_{px\text{-}ol}$ fractionations have been reported by Kyser et al. (Kyser et al. 1981) in a study that used conventional fluorination. These results were explained by open-system metasomatic processes (Gregory and Taylor 1986a, b) and called into question following the advent of laser

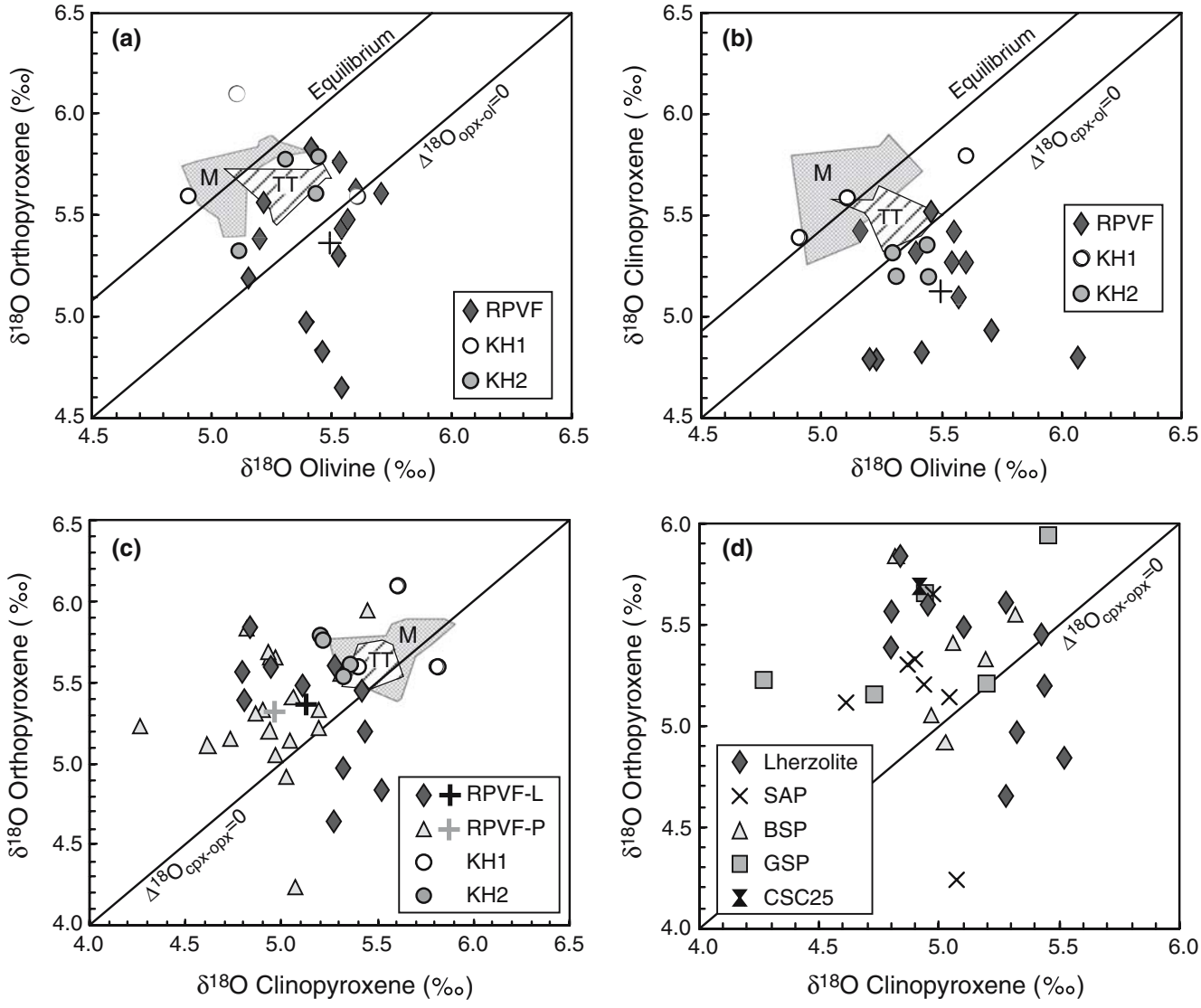

Fig. 3 Oxygen isotope compositions of mineral separates. **a** Orthopyroxene versus olivine, Rio Puerco lherzolite (this study). *M* global mantle average, *TT* The Thumb, $n = 12$ (Mattey et al. 1994). *KH1* Kilbourne Hole by conventional extraction (Kyser et al. 1981); *KH2* Kilbourne Hole by laser fluorination (this study). Equilibrium line shows typical $\Delta^{18}O_{opx\text{-}ol}$ for spinel lherzolite xenoliths worldwide. **b** Clinopyroxene versus olivine in lherzolites, symbols as in **a**. **c** Orthopyroxene versus clinopyroxene for lherzolites and pyroxenites. *RPVF-L* Rio Puerco lherzolite, *RPVF-P* Rio Puerco pyroxenite (this study). Large crosses represent averages of RPVF data. Other symbols as in **a**. **d** Orthopyroxene versus clinopyroxene for lherzolites and pyroxenites from the RPVF, by spinel type. *SAP* spinel-absent pyroxenite; *GSP* green spinel-bearing pyroxenite; *BSP* black spinel-bearing pyroxenite. *CSC25* brown spinel-bearing pyroxenite

fluorination. Mattey et al. (1994) reported only positive $\Delta^{18}O_{px\text{-}ol}$ fractionations in a study of 76 mantle xenoliths and Chazot et al. (1997) found only positive $\Delta^{18}O_{px\text{-}ol}$ fractionations in a study of hydrous and anhydrous xenoliths. More recent workers (Deines and Haggerty 2000; Orr and Luth 2000; Zhang et al. 2000; Zhang et al. 2001) have observed oxygen isotope disequilibrium in kimberlite-hosted polymict peridotites and eclogites, which was attributed to metasomatism by fluids related to the entraining magma.

Metasomatism by a low $\delta^{18}O$ fluid or melt is the most reasonable explanation for the negative $\Delta^{18}O_{px\text{-}ol}$ fractionations and unusually low $\delta^{18}O$ pyroxenes in RPVF xenoliths. Features consistent with metasomatism, such as fluid inclusions and reactions involving melt, are abundant in the pyroxenes, but rare in olivine from the RPVF. Therefore, metasomatism may have preferentially affected pyroxenes, with low $\delta^{18}O$ infiltrating fluids exploiting crystallographic pathways along exsolution lamellae and cleavage planes. Also, oxygen diffusion in pyroxene is ~2 orders of magnitude faster than in olivine (Farver 1989; Rosenbaum et al. 1994b). Preferential metasomatic alteration of pyroxenes and accompanying larger variability in pyroxene $\delta^{18}O$ values has been noted in lherzolites (Mattey et al. 1994) and eclogite xenoliths (Deines and Haggerty 2000).

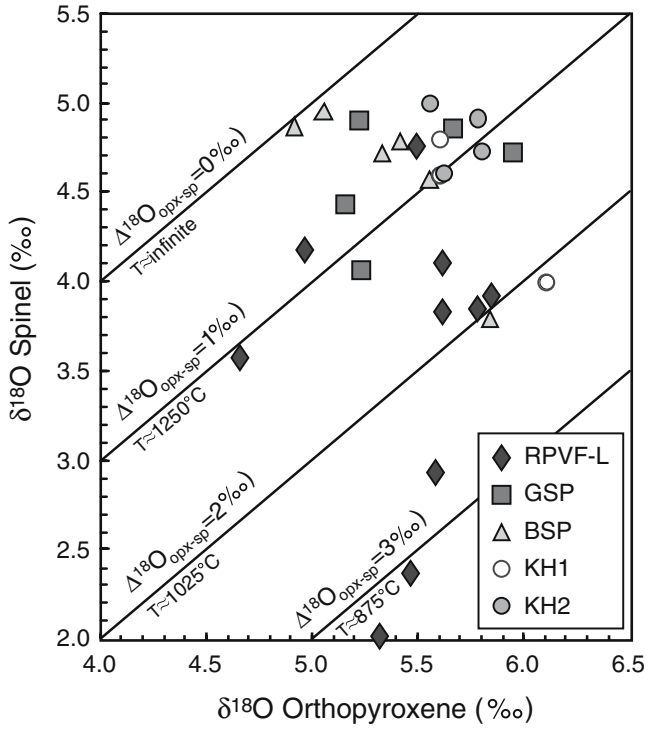

Fig. 4 $\delta^{18}O$ of spinel versus olivine for lherzolites and pyroxenites from the RPVF and Kilbourne Hole. Abbreviations as in Fig. 3d. Temperature-dependent equilibrium fractionations from Zheng (1991, 1993)

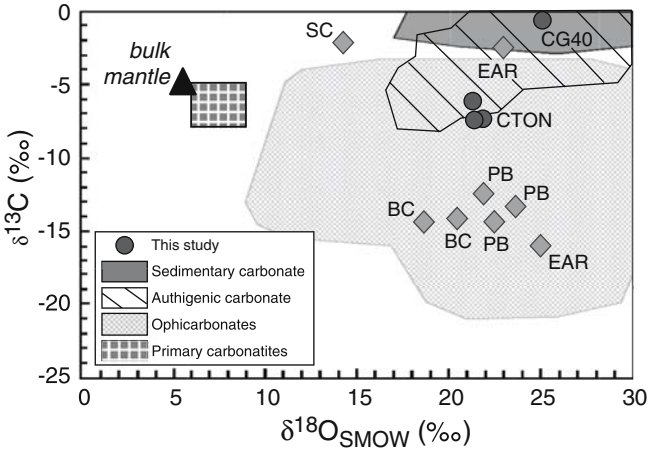

Fig. 5 $\delta^{18}O$ versus $\delta^{13}C$ for calcite in mantle xenoliths and other carbonate reservoirs. *CTON* Cerrito Negro (this study); *CG*40 Cerro de Guadalupe (this study); *PB* Pannonian Basin (Demény et al. 2004); *EAR* East African Rift (Lee et al. 2000); *BC* Big Creek, Sierra Nevada (Ducea et al. 2005); *SC* Lac de Gras, Slave Craton (van Achterbergh et al. 2002). Bulk mantle from Harmon and Hoefs (1995) and Deines (2002). Authigenic carbonate compositions from the southwestern U.S. from Quade et al. (1989), Wang et al. (1996), and Mack et al. (2000). Ophicarbonate compositions from Jedrysek and Sachanbinski (1994). Data for sedimentary carbonate reservoirs after Arthur et al. (1983)

The 1.0‰ range in $\delta^{18}O$ values for the pyroxenes suggests variable fluid-rock ratios, or varying degrees of reequilibration with the infiltrating fluid/melt. The low $\delta^{18}O$ clinopyroxenes and disequilibrium $\Delta^{18}O_{px\text{-}ol}$ fractionations in the Kilbourne Hole xenoliths are also most easily explained by preferential metasomatic alteration of clinopyroxene by an isotopically light fluid.

Interaction with the host basalts cannot explain the low $\delta^{18}O$ values of the pyroxenes. The RPVF basalts range in $\delta^{18}O$ from +5.0 to +7.0‰, with most volcanic necks falling within a more limited range of +5.6 to +6.4‰ (Hallett 1994). The basalts from four of the volcanic necks hosting xenoliths chosen for this study have the following $\delta^{18}O$ values: Cerro de Guadalupe (+6.4‰), Cerro de Santa Rosa (+6.4‰), Cerro Vacio (+6.3‰), and Cerro Negro (+6.2‰) (Hallett 1994). At temperatures in excess of 900°C, $\delta^{18}O_{basalt\text{-}cpx}$ fractionations should be less than 0.5‰ (Matthews et al. 1998; Zhao and Zheng 2002), so pyroxenes in equilibrium with the host basalts from these volcanic necks would have $\delta^{18}O$ values above +5.7‰, which was not observed. Thus, the metasomatic event causing isotopic disequilibrium must have occurred prior to entrainment within the host basalt.

The pyroxenites have unusually low pyroxene $\delta^{18}O$ values and commonly show isotopic disequilibrium between the two pyroxenes (Fig. 3c, d), suggesting a metasomatic history similar to that of the lherzolites, by interaction by low $\delta^{18}O$ fluids. On average, the pyroxenites pyroxene $\delta^{18}O$ values are less than 0.1‰ lower than those in lherzolites. Bulk rock and clinopyroxene major element compositions suggest that the RPVF pyroxenites formed from a combination of basaltic melt, lherzolitic mantle, and a Ca-rich carbonatite component (Porreca 2005). The basaltic and carbonatitic components in the pyroxenites in the RPVF could be derived from subducted oceanic crust (Porreca 2005), which would also provide a source for low $\delta^{18}O$ melts. Taylor et al. (2003) interpreted an origin for pyroxenite xenoliths from the Obnazhennaya kimberlite, Yakutia by a similar model involving mixing of slab-derived silicate and carbonatite melts and lherzolite to reconcile major element, Eu, and oxygen isotope geochemistries.

Spinel $\delta^{18}O$ values are markedly different between the lherzolites and pyroxenites (Fig. 4). Brown spinels in the lherzolites range in $\delta^{18}O$ from +2.0 to +4.8‰, although most samples fall within a restricted range of +3.8 to +4.2‰. For the lherzolites spinels have $\delta^{18}O$ values of $+4.0 \pm 0.2$‰ and a $\Delta^{18}O_{sp\text{-}ol}$ fractionations consistent with equilibrium temperatures of 875–1,050°C, using the fractionation factors of Zheng (1991, 1993). These temperature estimates agree well with those obtained by two-pyroxene thermometry (900–1,000°C, Porreca 2005). The lowest spinel $\delta^{18}O$ values are found only in xenoliths from Cerrito Negro and Cerro de Guadalupe, two volcanic necks with abundant textural evidence for metasomatism. Spinel in these xenoliths is more likely to have been altered by a low $\delta^{18}O$ fluid.

Spinels in pyroxenites have a mean $\delta^{18}O$ of +4.7‰, with most $\Delta^{18}O_{px\text{-}sp}$ fractionations suggesting temperatures above 1,200°C (Zheng 1991, 1993). However, reaction margins surrounding spinel in pyroxenites are

typical of disequilibrium textures, and the temperatures are hotter than those obtained by two-pyroxene thermometry on the pyroxenites (950–1,145°C, Porreca 2005). Nevertheless, both cation exchange thermometry and $\Delta^{18}O_{px\text{-}sp}$ fractionations are consistent with pyroxenites equilibrating at temperature 200°C hotter than the lherzolites. Two black spinel peridotites preserve relict garnets in a reaction texture to black spinel, clinopyroxene, orthopyroxene and glass, a reaction facilitated by heating and melt interaction, so it is reasonable that these samples were indeed at high temperatures. Spinels in BSPs and GSPs have similar $\delta^{18}O$ values, and textural observations suggest that green spinels are a product of black spinels and are formed with a melt phase (this is especially apparent in sample CTON9). Two of the Cerro Vacio GSPs have lower spinel $\delta^{18}O$ values ($+4.1$ and $+4.4‰$), and pyroxenes riddled with fluid inclusions, indicating a high fluid-rock ratio for metasomatism by a low $\delta^{18}O$ fluid.

Most mantle-derived basalts and peridotite xenoliths show a narrow range of $\delta^{18}O$ values from $+5.5$ to $+5.9‰$ (Mattey et al. 1994; Harmon and Hoefs 1995), and lower $\delta^{18}O$ values are assumed to indicate a component derived from subducted crust (e.g., MacGregor and Manton 1986, Eiler 2001and references therein). Altered oceanic crust has a wide range of $\delta^{18}O$ values from $+2‰$ to greater than $14‰$, depending on the temperature of hydrothermal exchange with seawater (Muehlenbachs 1986). This large range in $\delta^{18}O$ is preserved in kimberlite-hosted eclogite xenoliths (MacGregor and Manton 1986; Ongley et al. 1987; Neal et al. 1990; Snyder et al. 1995). Incorporation of previously subducted altered oceanic crust into the source regions in the mantle has been proposed as an explanation for low $\delta^{18}O$ values in phenocrysts in ocean island basalts and mid-ocean ridges with no clear geographic link to subduction (Eiler et al. 1997; Cooper et al. 2004; Demény et al, 2004; Xia et al. 2004), although others have suggested that crustal assimilation is the most common mechanism for shifting $\delta^{18}O$ values from their normal mantle value (Eiler 2001). In the case of the xenoliths under the western United States, $\delta^{18}O$ values that are lower than normal mantle strongly argue for altered oceanic crust as the cause of the shift. Crustal contamination would almost invariably cause an increase in the $\delta^{18}O$ value the xenolith protolith. Altered oceanic crust is the most likely method to create a low $\delta^{18}O$ source region for metasomatizing fluids and melts beneath the RPVF.

High $\delta^{18}O$ calcite

The carbonates in the RPVF xenolith suite provide an intriguing opportunity to investigate the origin of carbonatite melts, the composition of metasomatic fluids and the timing of their infiltration. Carbonates in mantle xenoliths have been reported from many tectonic settings globally, including continental rifts (Ionov 1998; Lee et al. 2000) and subduction zones (Laurora et al. 2001; Demény et al. 2004), but have been reported from only two localities in southwestern North America. Carbonates occur as inclusions in garnet in peridotite xenoliths from the Navajo volcanic field of the Colorado Plateau (McGetchin and Besançon 1973; Hunter and Smith 1981; Smith 1987), and as globules and veins in peridotite xenoliths from Big Creek, Sierra Nevada (Ducea et al. 2005). Textural evidence suggests that the calcite in the Cerrito Negro pyroxenites formed in the mantle prior to eruption. Individual calcite grains, both included in clinopyroxene and in the matrix, show pronounced Mn zoning and contain bands of silicate melt inclusions along the growth zones. Additionally, the calcite inclusions in clinopyroxene are intergrown with and contain inclusions of orthopyroxene (Fig. 2d, e), suggesting cotectic crystallization of the two phases (Wyllie and Lee 1998). Minerals such as zeolites, which would be diagnostic of surficial alteration, are absent. Based on the textural and compositional evidence, we thus interpret the Cerrito Negro calcites and their $\delta^{18}O$ values to be of mantle origin, in accord with other recent studies reporting high $\delta^{18}O$ carbonates in xenoliths (Demény et al. 2004; Ducea et al. 2005).

The high $\delta^{18}O$ values of the calcite must have originally equilibrated in a near-surface environment and been brought to the mantle during subduction. $\delta^{18}O$ values above $+20‰$ are limited to a few rock types present in oceanic crust, including most calcareous sediments (marls), ophicarbonates (carbonate veins in serpentinites), and altered pillow basalts (Staudigel et al. 1981; Jedrysek and Sachanbinski 1994). Oceanic crust subducted to 70 km has been shown to preserve its original oxygen isotope composition (Cartwright and Buick 2000; Miller et al. 2001), and $\delta^{18}O$ values up to $+17‰$ of coesite inclusions in diamondiferous eclogite xenoliths have been interpreted as evidence for a sedimentary origin (Schulze et al. 2003).

The $\delta^{13}C$ values are ambiguous in distinguishing among the possible sources for the isotopically distinct reservoir of carbonate in the mantle. Most marine carbonates have higher $\delta^{13}C$ ($\sim 0‰$), whereas reduced organic carbon has an average $\delta^{13}C$ of $-23‰$ (Arthur et al. 1983). The $\delta^{13}C$ values of ophicarbonates range from -5 to $-20‰$ (Jedrysek and Sachanbinski 1994). The Rio Puerco xenolith RPVF calcites have O and C isotopic compositions similar to ophicarbonates, but also could also be explained by a mixture of subducted calcareous material and reduced organic carbon (Fig. 5). Subducted carbonaceous sediments have been interpreted as the source for high $\delta^{18}O$ ($+20$ to $+22‰$) calcites in the Pannonian Basin and the Big Creek lherzolite xenoliths (Demény et al. 2004; Ducea et al. 2005). The high $\delta^{18}O$ value ($+14‰$) of carbonate globules in the Slave craton kimberlites represents quenched melt derived from partial melting of a carbonated peridotite with a component of subducted crust (van Achterbergh et al. 2002).

Tectonic model for metasomatism of the RPVF lithosphere

Subduction is the sole mechanism for introducing both low and high $\delta^{18}O$ isotopic reservoirs into the mantle to provide a source region for the metasomatic fluids beneath the RPVF. The major subduction events affecting the southwest United States lithosphere are associated with continental accretion in the Paleoproterozoic and the late Cretaceous to early Tertiary subduction of the Farallon plate beneath western North America (Fig. 6). Regardless of which event was the primary source of the subduction component, an isotopically distinct reservoir must have been preserved in the mantle for an extended period of time prior to metasomatism. The RPVF necks sample different locations across the Jemez lineament, a Proterozoic structure that may have been a subduction zone with a northwest–southeast vergence direction (Dueker et al. 2001). However, no systematic variations in oxygen isotope composition with geographic position in the RPVF are observed, as might be expected if fluids were derived from Proterozoic subduction. Additionally,

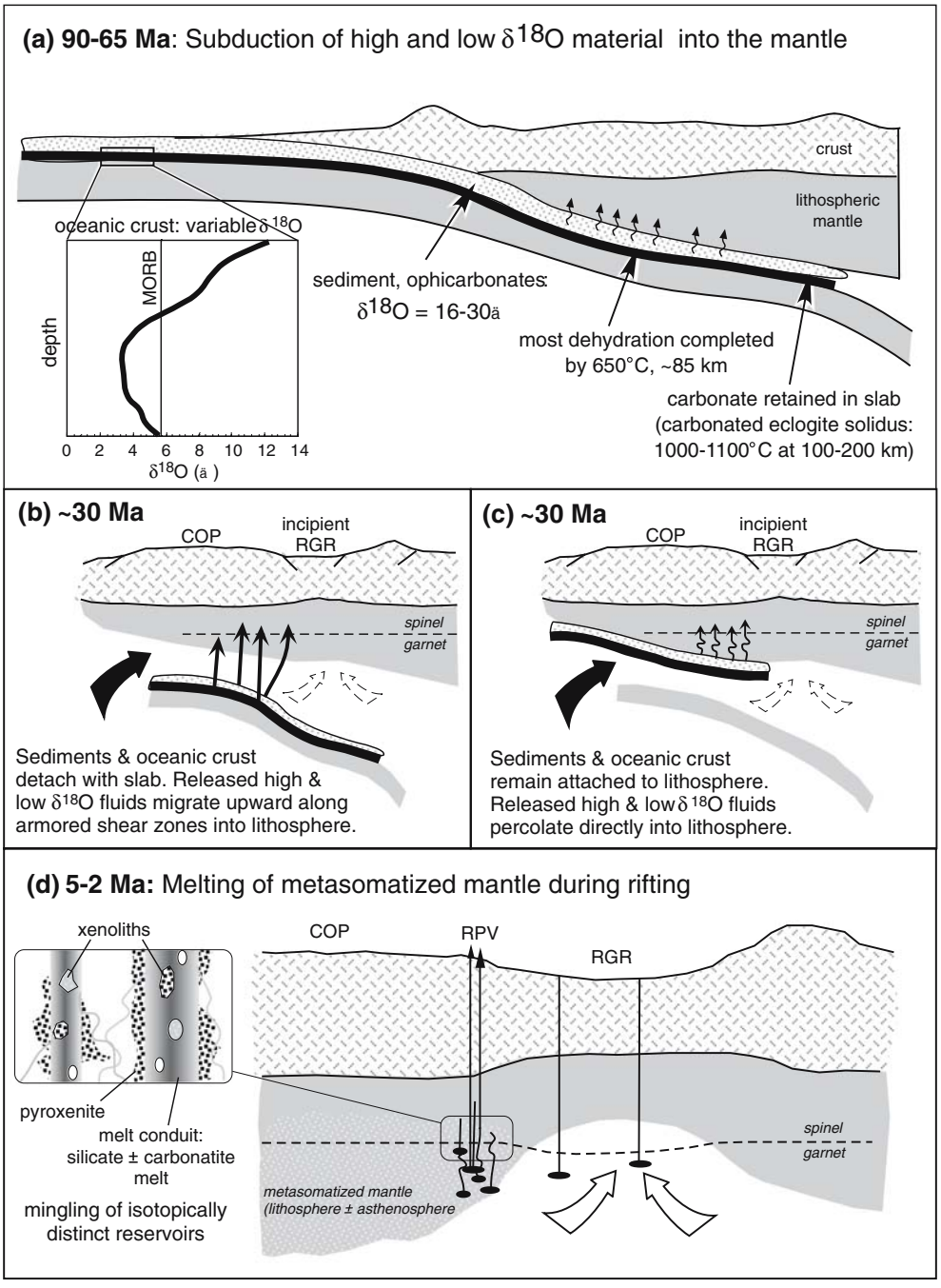

Fig. 6 Tectonic cartoons illustrating possible mechanisms for producing and maintaining discrete high and low $\delta^{18}O$ mantle domains. **a** Possible Cretaceous subduction geometry beneath western U.S., based on model of Humphreys et al. (2003). Altered oceanic crust shows $\delta^{18}O$ values that are perturbed relative to MORB and that vary systematically with depth (Gregory and Taylor 1981); subducted sedimentary rocks and ophicarbonates have high $\delta^{18}O$. Most dehydration reactions will occur in the early stages of subduction, but carbonate can be retained to higher pressures and temperatures. Dehydration and decarbonation will release fluids of differing $\delta^{18}O$ over a large depth interval. **b** and **c** Two possible models for generation of anomalous $\delta^{18}O$ basaltic ± carbonatitic melts from carbonated eclogite following slab detachment and asthenospheric upwelling. **b** Oceanic crust and subducted sediments detach with slab. Partial melts ascend to lithosphere in discrete shear zones, thus preserving their $\delta^{18}O$ signature. **c** Oceanic crust and sediments underplate continental lithosphere. Heating from below triggers partial melting, and melts infiltrate directly into lithosphere. **d** Rio Grande rifting triggers partial melting of metasomatized mantle. Melt ascent and melt-wallrock interactions result in mingling of isotopically distinct reservoirs. Short timescales of interaction prevent isotopic equilibration

the isotopic characteristics of the RPVF xenoliths are shared by those over 300 km to the south at Kilbourne Hole, which also has clinopyroxenes with low $\delta^{18}O$ values that can be explained by metasomatism by slab-derived isotopically light fluids or melts. We thus favor introduction of the subduction component during flat-slab subduction of the Farallon plate.

Tertiary subduction of the Farallon slab extended at least to the central Colorado Plateau, where diatremes host eclogite xenoliths with Tertiary-age zircons both directly from the Farallon slab (Usui et al. 2003) and as products of dehydration of this slab (Smith et al. 2004). Seismic images show a foundering slab now below the Great Plains (Van der Lee and Nolet 1997; Bunge and Grand 2000). During the mid-Tertiary, the lithospheric mantle extended to 150–200 km (Humphreys and Dueker 1994), and may have been in direct contact with the subducted slab (Fig. 6a) (Humphreys et al. 2003).

At a depth of 175 km, dehydration of subducted sediment and metabasalt occurs between 600 and 800°C, and dehydration of serpentinites is largely completed by 625°C (Ulmer and Trommsdorff 1995). Ophicarbonate undergoes decarbonation at somewhat higher temperatures (Kerrick and Connolly 1998), and the solidus of carbonated eclogite is reached at 1,100–1,300°C (Yaxley et al. 1998; Hammouda 2003; Dasgupta et al. 2004), and of carbonated peridotite at 1,250–1,350°C (Canil and Scarfe 1990; Dalton and Presnall 1998).

Given the above constraints, hydrous and carbonate phases could have remained in the slab beneath much of southwestern North America, including the RPVF and Kilbourne Hole, for an indefinite period of time. Fluids or melts ultimately released from the slab into the overlying mantle could have had $\delta^{18}O$ values that were either higher or lower than typical mantle depending on their origin. During flat slab subduction, the temperature beneath the Colorado Plateau was likely sufficient to dehydrate metabasalt and sediment, yet still too cold to release of CO_2 from other parts of the slab. Thus, the low $\delta^{18}O$ portion of the slab may have been unaffected by heating while the upper portion of underwent dehydration (Fig. 6a). Subsequent detachment of the slab and the onset of rifting would have led to asthenospheric upwelling and widespread heating in southwestern North America in the mid-Tertiary (Fig. 6b, c) (Humphreys et al. 2003). Mantle xenoliths from the Colorado Plateau record heating from $\leq$ 950°C to over 1,150°C between 25 and 30 Ma, confirming the Tertiary temperature rise (Smith and Barron 1991). This heating likely caused partial melting of the crustal portion of the slab, regardless of whether that crust was part of the detached slab (Fig. 6b) or remained attached to the overlying continental lithosphere (Fig. 6c). The temperatures were likely sufficiently high to generate both low $\delta^{18}O$ basaltic melts from altered oceanic crust and high $\delta^{18}O$ carbonatitic melts or carbonic fluids from carbonated eclogite and/or ophicarbonate.

The potential for melt immiscibility (Lee and Wyllie 1997; Brooker 1998) and the high viscosity contrast between carbonate melt and silicate melt provide effective mechanisms for physical separation of the two melt types and preserve isotopic differences between them. Alternatively, low $\delta^{18}O$ basaltic melt and high $\delta^{18}O$ carbonatite melt may have been released at different temperatures and times, thereby allowing them to preserve their isotopic composition. In this case, isotopically and chemically distinct melts would remain separate during ascent to the spinel-facies mantle, regardless of conditions governing immiscibility.

Preservation of both high and low $\delta^{18}O$ reservoirs in the mantle can only be achieved if there was minimal interaction with surrounding mantle as the melt or fluid moved upward into the mantle of the spinel facies. This could be accomplished if melt/fluid ascent to the spinel facies occurred along discrete fractures (Fig. 6b) (Hacker et al. 2003). Reaction margins at the sides of the fractures would armor the ascending melt/fluid from interaction with the surrounding mantle. This mechanism has been shown to hinder vein-wallrock interaction in metamorphosed schists and to preserve fluid $\delta^{18}O$ compositions (Rye and Bradbury 1988; Cartwright and Buick 2000). It is also a likely mechanism for formation of the pyroxenite xenoliths, which show chemical and petrographic evidence for reaction between spinel lherzolite and basaltic melt $\pm$ carbonatite melt.

Xenoliths from Kilbourne Hole, which is located within the Rio Grande Rift, also show evidence for metasomatism by low $\delta^{18}O$ fluids; however, xenoliths from The Thumb, in the Colorado Plateau, show no evidence for interaction with low $\delta^{18}O$ fluids. The lack of metasomatism in the Colorado Plateau samples suggests that low $\delta^{18}O$ fluid or melts either were never released from the slab in this region—due to cooler temperatures—or, once generated, were unable to infiltrate the lithosphere.

Diffusion constraints on timing of metasomatism

Both the lherzolites and the carbonated pyroxenites from the RPVF exhibit isotopic disequilibrium between coexisting minerals. In previous studies, oxygen isotope disequilibrium in mantle peridotites and eclogites had been interpreted as indicative of interaction with fluids or melts associated with entrainment (Deines and Haggerty 2000; Orr and Luth 2000; Zhang et al. 2000, 2001). Using oxygen diffusion data, the occurrence and extent of isotopic disequilibrium can provide an estimate on the timing of metasomatism.

The conditions for instilling negative $\Delta^{18}O_{px\text{-}ol}$ fractionations in the mantle have been previously explored in detail by Rosenbaum et al. (1994b) for many combinations of fluid compositions and mineral proportions using an open system exchange model with different diffusion rates, grain sizes, and changing isotopic compositions of both phases. Rosenbaum et al. (1994b) showed that diffusion of oxygen in olivine and pyroxenes at mantle temperatures is sufficiently rapid

that negative $\Delta^{18}O_{px\text{-}ol}$ fractionations are unlikely to be preserved after ~10,000 years. However, the Rosenbaum et al. (1994b) models were run at hotter temperatures (1,200°C) than are appropriate for the RPVF lherzolites (900–1,000°C, Porreca 2005). Extrapolation of the Rosenbaum et al. (1994b) models to these temperatures suggests that isotopic disequilibrium in the RPVF lherzolites may have persisted for 1–2 orders of magnitude longer (perhaps up to 1 M.y. before eruption).

In previous studies reporting isotopic disequilibrium between carbonates and host silicate minerals in mantle xenoliths, carbonate infiltration was assumed to have occurred less than 1 M.y. prior to eruption (van Achterbergh et al. 2002; Demény et al. 2004; Ducea et al. 2005), although details regarding how this time constraint was obtained are not well documented. Calcite grains are hosted both as inclusions within clinopyroxene, which composes the bulk of the pyroxenites, and as distinct matrix grains. At mantle temperatures, oxygen self diffusion rates in calcite are 2–6 orders of magnitude faster than in clinopyroxene (Connolly and Muehlenbachs 1988; Farver 1989, 1994; Elphick and Graham 1990; Ryerson and McKeegan 1994; Labotka et al. 2000; Ingrin et al. 2001), so that no diffusional gradients should exist within the calcite itself. Models using the assumption of fast grain boundary diffusion suggest that the diffusion rate of oxygen in calcite should determine its $\delta^{18}O$ value, as the faster diffusing calcite is surrounded by a large volume of slowly diffusing clinopyroxene with extremely high surface area (Eiler et al. 1992; Jenkin et al. 1994). In either case, the clinopyroxene is modally dominant and the $\delta^{18}O$ value of the calcite is determined using the equation of Crank (1975) for a semi-infinite medium adjacent to a plane of constant composition:

$$\delta^{18}O_{cc}(t) = \delta^{18}Occ,eqm + (\delta^{18}O_{cc,i} - \delta^{18}Occ,eqm) \times \mathrm{erf}\left(\frac{r}{2\sqrt{Dt}}\right), \quad (1)$$

where $\delta^{18}O_{cc,eqm}$ is the $\delta^{18}O$ value of calcite in equilibrium with clinopyroxene for a given temperature, $\delta^{18}O_{cc,i}$ is the measured $\delta^{18}O$ value of calcite, r is the radius of calcite (in m), t is time (s), and D is the oxygen diffusion coefficient (m^2/s). $\delta^{18}O_{cc,eqm}$ was determined by calculating $\delta^{18}O_{cc\text{-}cpx}$ using the fractionation factor ($a_{cc\text{-}cpx}$) of 2.37 for a given temperature (T in K) (Chiba et al. 1989) where the fractionation between the two phases is given by

$$1000 \ln \alpha = \frac{a \times 10^6}{T^2} \quad (2)$$

and

$$\alpha_{cc-cpx} = \frac{1000 + \delta^{18}O_{cc}}{1000 + \delta^{18}O_{cpx}}. \quad (3)$$

Parameters chosen for this calculation use the oxygen isotope results from this study ($\delta^{18}O_{cpx} = +5.0‰$, $\delta^{18}O_{cc,init} = +21.5‰$), a typical calcite radius from the carbonate-bearing Cerrito Negro xenoliths ($r = 0.5$ mm), and an equilibration temperature of 1,100°C (in accord with cation thermometry of CTON-2 and CTON-7; Porreca 2005), which corresponds to an equilibrium $\Delta^{18}O_{cc\text{-}cpx}$ fractionation of +1.26‰.

If oxygen diffusion rates are not limited by exchange at the grain boundaries, as suggested by Eiler et al. (1992) and Jenkin et al. (1994), the diffusion coefficients for calcite determine the degree of exchange with the hosting clinopyroxene (Table 3). Pressure, cation composition, and the presence of water strongly affect the rate of oxygen diffusion in calcite (Kronenberg et al. 1984; Labotka et al. 2004). This study uses the results from the studies at 100 MPa by Farver (1994) and Labotka et al. (2000), for hydrous and anhydrous conditions, respectively. At this pressure, and presumably higher pressures as well, diffusion is accomplished through movement of individual O atoms, whereas migration of CO_3^{2-} anions is the dominant mechanism for diffusion in calcite at low pressures (Labotka et al. 2004). Using the anhydrous calcite diffusion rates at 1,100°C, $\delta^{18}O_{cc}$ values could remain above +20‰ for only 4 years and above +15‰ for only 14 years; calcite with an original $\delta^{18}O = +30‰$ would be reduced to its current isotopic composition in ~10 years (Table 3). Even for grain radii an order of magnitude larger than assumed here, exchange rates are extremely rapid. High $\delta^{18}O$ values of the calcite can thus only be preserved if carbonic melt was emplaced in the xenoliths very shortly before eruption, and therefore may have been part of the process that triggered the eruption.

Conclusions

Oxygen isotope geochemistry of the RPVF xenoliths record disequilibrium metasomatic processes that occurred immediately prior to eruption and entrainment at 4.5–2.0 Ma. Low $\delta^{18}O$ values in the pyroxenes are consistent with interaction with a metasomatic component derived from subducted altered oceanic crust. Unusually high $\delta^{18}O$ calcite in the RPVF xenoliths likely crystallized from carbonatite melts derived from melting of subducted ophicarbonate and/or carbonated eclogite. The Farallon slab, subducted in the late Cretaceous and early Tertiary, is favored as the source for melts derived from subducted crust. The mobilization of slab-derived melts is interpreted to result from subsequent rift-related heating and asthenospheric upwelling, during which the low $\delta^{18}O$ melt and lesser volumes of high $\delta^{18}O$ carbonatite melt were mobilized and ascended to the spinel-facies mantle. Pyroxenes within lherzolites were preferentially affected by metasomatism, whereas olivine shows little petrographic or isotopic evidence for interaction with ascending melts or fluids. Pyroxenites formed via extensive interaction of spinel lherzolite with

Table 3 Experimentally determined diffusion coefficients for oxygen in clinopyroxene and calcite

		E (kJ/mol)	D_0 (m^2/s)	D (m^2/s) at 1,100°C	Years to $\delta^{18}O = +20‰$	Years to $\delta^{18}O = +15‰$	Years from $\delta^{18}O = +30‰$
O diffusion in diopside							
Connolly and Muehlenbachs (1988)	a	404	6.30E-04	2.69E-19	5,396	23,299	17,443
Farver (1989) parallel c	h	226	1.50E-10	3.79E-19	3,833	16,551	12,391
Farver (1989) perpendicular c	h	226	2.80E-12	7.07E-21	205,340	866,400	663,780
Elphick and Graham (1990)	h	351	9.00E-07	3.99E-20	36,379	157,080	117,600
Ryerson and McKeegan (1994)	a	457	4.30E-04	1.77E-21	820,850	3,544,300	2,653,500
Ingrin et al. (2001) a,c	a	259	1.00E-10	1.40E-20	103,530	447,040	334,680
Ingrin et al. (2001) b	a	323	1.58E-09	8.16E-22	1,777,800	7,676,200	5,746,800
O diffusion in calcite, 100 MPa							
Farver (1994)	h	173	7.00E-09	1.83E-15	0.8	3.4	2.6
Labotka et al. (2000)	a	242	7.50E-07	4.66E-16	3.1	13.4	10.1

Results are for oxygen self-diffusion through a semi-infinite reservoir of clinopyroxene with $\delta^{18}O = +5.0‰$ at 1,100°C for a 1 mm calcite of $\delta^{18}O = +21.5‰$ to decrease to $+20‰$ and $+15‰$, and the time for calcite of original $\delta^{18}O = +30‰$ to be reduced to its current composition of $+21.5‰$

a experiment run under anhydrous conditions; *h* experiment run under hydrous conditions

both low $\delta^{18}O$ silicate melt and high $\delta^{18}O$ carbonatitic melt, probably along the margins of melt conduits. The lack of isotopic and textural reequilibration within the pyroxenites indicates that the mantle sampled by the RPVF underwent metasomatism immediately prior to entrainment in the host basalts. However, direct interaction with the host basalts is precluded by the fact that the basalts were derived from garnet-facies mantle (Hallett 1994) and the xenoliths represent spinel-facies mantle. Xenoliths from Kilbourne Hole show similar evidence for isotopic disequilibrium. Metasomatic modification of the mantle immediately prior to eruption thus appears to be a widespread phenomenon in the Rio Grande rift, and likely played a role in triggering partial melting within the deeper source region for the host magmas.

Acknowledgments Courtney Porreca, Kym Samuels, Adrian Brearley, Caitlin Callahan, and Mousumi Roy generously shared data and had many stimulating discussions with us. We are grateful to Mihai Ducea and Attila Demény for journal reviews and to Doug Smith for additional comments on the manuscript. Financial support was provided by NSF grant EAR-0229238.

References

Aldrich MJ, Laughlin AW (1984) A model for the tectonic development of the southeastern Colorado Plateau boundary. J Geophys Res 89:10207–10218

Arthur M, Anderson T, Kaplan I (1983) Stable isotopes in sedimentary geology. SEPM Short Course vol 10, pp 432

Atwater T (1970) Implications of plate tectonics for the Cenozoic tectonic evolution of western North America. Geol Soc Amer Bull 81:3513–3536

Bird P (1988) Formation of the Rocky Mountains, western United States: a continuum computer model. Science 239:1501–1507

Brooker R (1998) The effect of CO_2 saturation on immiscibility between silicate and carbonate liquids: an experimental study. J Petrol 39:1905–1915

Bunge HP, Grand SP (2000) Mesozoic plate-motion history below the northeast Pacific Ocean from seismic images of the subducted Farallon slab. Nature 405:337–340

Bussod GYA, Williams DR (1991) Thermal and kinematic model of the southern Rio Grande Rift: inferences from crustal and mantle xenoliths From Kilbourne Hole, New Mexico. Tectonophysics 197:373–389

Callahan C, Geissman JW, Brearley AJ, Selverstone J (2004) Characterization of magnetic properties and magnetic mineralogy of mantle xenoliths from the Rio Puerco volcanic field, New Mexico. Geol Soc Amer Prog Abs 36:146

Canil D, Scarfe CM (1990) Phase relations in peridotite + CO_2 systems to 12 GPa- implications for the origin of kimberlite and carbonatite stability in the Earth's upper mantle. J Geophys Res 95:15805–15816

Cartwright I, Buick I (2000) Fluid generation, vein formation and the degree of fluid–rock interaction during decompression of high-pressure terranes: the Schistes Lustrés, Alpine Corsica, France. J Metamorph Geol 18:607–624

Cather S (1999) Implications of Jurassic, Cretaceous, and Proterozoic piercing lines for Laramide oblique-slip faulting in New Mexico and rotation of the Colorado Plateau. Geol Soc Amer Bull 111:849–868

Chazot G, Lowry D, Menzies M, Mattey D (1997) Oxygen isotopic composition of hydrous and anhydrous mantle peridotites. Geochim Cosmochim Acta 61:161–169

Chiba H, Chacko T, Clayton R, Goldsmith J (1989) Oxygen isotope fractionations involving diopside, forsterite, magnetite, and calcite: application to geothermometry. Geochim Cosmochim Acta 53:2985–2995

Condie KC (1986) Geochemistry and tectonic setting of early Proterozoic supracrustal rocks in the southwestern United States. J Geol 94:845–864

Coney P, Reynolds S (1977) Flattening of the Farallon slab. Nature 270:403–406

Connolly C, Muehlenbachs K (1988) Contrasting oxygen diffusion in nepheline, diopside, and other silicates and their relevance to isotopic systematics in meteorites. Geochim Cosmochim Acta 52:1585–1591

Cooper K, Eiler JM, Asimow P, Langmuir C (2004) Oxygen isotope evidence for the origin of enriched mantle beneath the mid-Atlantic ridge. Earth Plan Sci Lett 220:297–316

Crank J (1975) The mathematics of diffusion. Clarendon, Oxford p 414

Dalton JA, Presnall DC (1998) Carbonatitic melts along the solidus of model lherzolite in the system $CaO–MgO–Al_2O_3–SiO_2–CO_2$ from 3 to 7 GPa. Contrib Mineral Petrol 131:123–135

Dasgupta R, Hirschmann MM, Withers AC (2004) Deep global cycling of carbon constrained by the solidus of anhydrous, carbonated eclogite under upper mantle conditions. Earth Plan Sci Lett 227:73–85

Deines P (2002) The carbon isotope geochemistry of mantle xenoliths. Earth-Sci Rev 58:247–278
Deines P, Haggerty S (2000) Small-scale oxygen isotope variations and petrochemistry of ultradeep (> 300 km) and transition zone xenoliths. Geochim Cosmochim Acta 64:117–131
Demény A, Vennemann TW, Hegner E, Nagy G, Milton JA, Embey-Isztin A, Homonnay Z, Dobosi G (2004) Trace element and C–O–Sr–Nd isotope evidence for subduction-related carbonate-silicate melts in mantle xenoliths (Pannonian Basin, Hungary). Lithos 75:89–113
Ducea M, Saleeby J, Morrison J, Valencia V (2005) Subducted carbonates, metasomatism of mantle wedges, and possible connections to diamond formation: an example from California. Am Mineral 90:864–870
Dueker K, Yuan H, Zurek B (2001) Thick Proterozoic lithosphere of the Rocky Mountain region. GSA Today 11:4–9
Dumitru T, Gans P, Foster D, Miller E (1991) Refrigeration of the western Cordilleran lithosphere during Laramide shallow-angle subduction. Geology 19:1145–1148
Eiler JM (2001) Oxygen isotope variations of basaltic lavas and upper mantle rocks. In: Valley JW, Cole DR (eds) Stable isotope geochemistry, Reviews Mineral Geochemistry vol 43. Mineral Soc Amer, Washington DC, pp 319–364
Eiler JM, Baumgartner LP, Valley JW (1992) Intercrystalline stable isotope diffusion—a fast grain-boundary model. Contrib Mineral Petrol 112:543–557
Eiler JM, Farley KA, Valley JW, Hauri E, Craig H, Hart SR, Stolper EM (1997) Oxygen isotope variations in ocean island basalt phenocrysts. Geochim Cosmochim Acta 61:2281–2293
Eiler JM, McInnes B, Valley JW, Graham CM, Stolper EM (1998) Oxygen isotope evidence for slab-derived fluids in the sub-arc mantle. Nature 393:777–781
Eiler JM, Schiano P, Kitchen N, Stolper EM (2000) Oxygen-isotype evidence for recycled crust in the sources of mid-ocean-ridge basalts. Nature 403:530–534
Elphick S, Graham CM (1990) Hydrothermal oxygen diffusion in diopside at 1 Kb, 900–1200°C, a comparison with oxygen diffusion in forsterite and constraints on oxygen isotope disequilibrium in peridotite nodules. Terra Abst 7:72
Farver JR (1989) Oxygen self-diffusion in diopside with application to cooling rate determinations. Earth Plan Sci Lett 92:386–396
Farver JR (1994) Oxygen self-diffusion in calcite—dependence on temperature and water fugacity. Earth Plan Sci Lett 121:575–587
Gao W, Grand SP, Baldridge WS, Wilson D, West M, Ni JF, Aster R (2004) Upper mantle convection beneath the central Rio Grande rift imaged by P and S wave tomography. J Geophys Res 109 DOI 10.1029/2003JB002743
Gregory RT, Taylor HP Jr (1981) An oxygen isotope profile in a section of Cretaceous oceanic crust, Samail ophiolite, Oman: evidence for ^{18}O buffering of the oceans by deep (> 5km) seawater-hydrothermal circulation at mid-ocean ridges. J Geophys Res 86:2737–2755
Gregory R, Taylor H (1986a) Non-equilibrium, metasomatic $^{18}O/^{16}O$ effects in upper mantle mineral assemblages. Contrib Mineral Petrol 93:124–135
Gregory R, Taylor H (1986b) Possible non-equilibrium oxygen isotope effects in mantle nodules, an alternative to the Kyser-O'Neil-Carmichael $^{18}O/^{16}O$ geothermometer. Contrib Mineral Petrol 93:114–119
Hacker BR, Peacock SM, Abers G, Holloway S (2003) Subduction factory 2. Are intermediate-depth earthquakes in subducting slabs linked to metamorphic dehydration reactions? J Geophys Res 108 DOI 10.1029/2001JB001129
Hallett RB (1994) Volcanic geology, paleomagnetism, geochronology, and geochemistry of the Rio Puerco necks, west-central New Mexico. PhD dissertation, New Mexico Institute of Mining and Technology, Socorro, p 340
Hallett RB, Kyle PR, McIntosh WC (1997) Paleomagnetic and Ar-40/Ar-39 age constraints on the chronologic evolution of the Rio Puerco volcanic necks and Mesa Prieta, west-central New Mexico: implications for transition zone magmatism. Geol Soc Amer Bull 109:95–106
Hammouda T (2003) High-pressure melting of carbonated eclogite and experimental constraints on carbon recycling and storage in the mantle. Earth Plan Sci Lett 214:357–368
Harmon RS, Hoefs J (1995) Oxygen isotope heterogeneity of the mantle deduced from global 18O systematics of basalts from different geotectonic settings. Contrib Mineral Petrol 120:95–114
Humphreys E, Dueker K (1994) Physical state of the western U.S. upper mantle. J Geophys Res 99:9635–9650
Humphreys E, Hessler E, Dueker K, Farmer CL, Erslev E, Atwater T (2003) How Laramide-age hydration of North American lithosphere by the Farallon slab controlled subsequent activity in the western United States. Internat Geol Rev 45:575–595
Hunter W, Smith D (1981) Garnet peridotite from Colorado Plateau ultramafic diatremes: hydrates, carbonates, and comparative geothermometry. Contrib Mineral Petrol 76:312–320
Hut G (1987) Consultants' group meeting on stable isotope reference samples for geochemical and hydrological investigations. International Atomic Energy Agency
Ingrin J, Pacaud L, Jaoul O (2001) Anisotropy of oxygen diffusion in diopside. Earth Plan Sci Lett 192:347–361
Ionov D (1998) Trace element composition of mantle-derived carbonates and coexisting phases in peridotite xenoliths from alkali basalts. J Petrol 39:1931–1941
Javoy M, Pineau F, Delorme H (1986) Carbon and nitrogen isotopes in the mantle. Chem Geol 57:41–62
Jedrysek MO, Sachanbinski M (1994) Stable isotope and trace element studies of vein ophicarbonates at Gogolow-Jordanow serpentinite massif (Poland)—a contribution to the origin of ophiaragonite and ophimagnesite. Geochem J 28:341–350
Jenkin G, Farrow C, Fallick A, Higgins D (1994) Oxygen isotope exchange and closure temperatures in cooling rocks. J Metamorph Geol 12:221–235
Karlstrom KE, Humphreys ED (1998) Persistent influence of Proterozoic accretionary boundaries in the tectonic evolution of southwestern North America: interaction of cratonic grain and mantle modification events. Rocky Mt Geol 33:161–179
Keller GR, Khan MA, Morgan P, Wendlandt RF, Baldridge WS, Olsen KH, Prodehl C, Braile LW (1991) A comparative-study of the Rio Grande and Kenya Rifts. Tectonophysics 197:355–371
Kerrick DM, Connolly JAD (1998) Subduction of ophicarbonates and recycling of CO_2 and H_2O. Geology 26:375–378
Kil Y, Wendlandt RF (2004) Pressure and temperature evolution of upper mantle under the Rio Grande Rift. Contrib Mineral Petrol 148:265–280
Kronenberg AK, Yund RA, Giletti BJ (1984) Carbon and oxygen diffusion in calcite: Effects of Mn content and PH_2O. Phys Chem Mineral 11:101–112
Kyser TK, O'Neil J, Carmichael ISE (1981) Oxygen isotope thermometry of basic lavas and mantle nodules. Contrib Mineral Petrol 77:11–23
Labotka TC, Cole DR, Riciputi LR (2000) Diffusion of C and O in calcite at 100 MPa. Am Mineral 85:488–494
Labotka TC, Cole DR, Riciputi LR, Fayek M (2004) Diffusion of C and O in calcite from 0.1 to 200 MPa. Am Mineral 89:799
Lassiter J, Hauri E (1998) Osmium-isotope variations in Hawaiian lavas: evidence for recycled oceanic lithosphere in the Hawaiian plume. Earth Plan Sci Lett 164:483–496
Laurora A, Mazzucchelli M, Rivalenti G, Vannucci R, Zanetti A, Barbieri MA, Cingolani CA (2001) Metasomatism and melting in carbonated peridotite xenoliths from the mantle wedge: the Gobernador Gregores case (Southern Patagonia). J Petrol 42:69–87
Lee CT, Rudnick RL, McDonough WF, Horn I (2000) Petrologic and geochemical investigation of carbonates in peridotite xenoliths from northeastern Tanzania. Contrib Mineral Petrol 139:470–484
Lee CT, Yin QZ, Rudnick RL, Jacobsen SB (2001) Preservation of ancient and fertile lithospheric mantle beneath the southwestern United States. Nature 411:69–73

Lee WJ, Wyllie PJ (1997) Liquid immiscibility between nephelinite and carbonatite from 1.0 to 2.5 GPa compared with mantle melt compositions. Contrib Mineral Petrol 127:1–16

Mack G, Cole D, Treviño L (2000) The distribution and discrimination of shallow authigenic carbonate in the Pliocene–Pleistocene Palomas Basin, southern Rio Grande Rift. Geol Soc Amer Bull 112:643–656

McCrea J (1950) On the isotopic chemistry of carbonates and a paleotemperature scale. J Chem Phys 18:849–857

MacGregor I, Manton WI (1986) Roberts Victor eclogites: ancient oceanic crust. J Geophys Res 91:14063–14079

Macpherson C, Hilton D, Day J, Lowry D, Grönvold K (2005) High $^{3}He/^{4}He$, depleted mantle and low-$\delta^{18}O$, recycled oceanic lithosphere in the source of central Iceland magmatism. Earth Plan Sci Lett 233:411–427

Mattey D, Lowry D, Macpherson C (1994) Oxygen isotope composition of mantle peridotite. Earth Plan Sci Lett 128:231–241

Matthews A, Stolper EM, Eiler JM (1998) Oxygen isotope fractionation among melts, minerals and rocks. Mineral Mag 62:971–972

McGetchin TR, Besançon J (1973) Carbonate inclusions in mantle-derived pyropes. Earth Plan Sci Lett 18:408–410

McMillan NJ (1998) Temporal and spatial magmatic evolution of the Rio Grande Rift. NM Geol Soc Guidebook 43:107–116

McMillan NJ, Dickin AP, Haag D (2000) Evolution of magma source regions in the Rio Grande rift, southern New Mexico. Geol Soc Am Bull 112:1582–1593

Miller J, Cartwright I, Buick I, Barnicoat A (2001) An O-isotope profile through the HP–LT Corsican ophiolite, France and its implications for fluid flow during subduction. Chem Geol 178:43–69

Muehlenbachs K (1986) Alteration of the oceanic crust and ^{18}O history of seawater. In: Valley JW, Taylor HP, O'Neil JR (eds) Stable isotopes in high-temperature geologic processes, vol 16. Mineral Soc Amer Reviews in Mineralogy, Washington D.C., pp 425–444

Neal CR, Taylor LA, Davidson JP, Holden P, Halliday AN, Nixon PH, Paces JB, Clayton RN, Mayeda TK (1990) Eclogites with oceanic crustal and mantle signatures from the Bellsbank kimberlite, South Africa, 2. Sr, Nd, and O isotope geochemistry. Earth Plan Sci Lett 99:362–379

Ongley J, Basu A, Kyser TK (1987) Oxygen isotopes in coexisting garnets, clinopyroxenes and phlogopites of Roberts Victor eclogites: implications for petrogenesis and mantle metasomatism. Earth Plan Sci Lett 99:362–379

Orr P, Luth R (2000) Petrology and oxygen-isotope geochemistry of the Yamba Lake kimberlite rocks, N.W.T. Can J Earth Sci 37:1053–1071

Padovani ER, Reid M (1989) Field guide to Kilbourne Hole maar, Doña Ana County, New Mexico. NM Bur Mines Mineral Res Memoir 46:174–179

Pearson DG, Davies G, Nixon P, Greenwood P, Mattey D (1991) Oxygen isotope evidence for the origin of pyroxenites in the Beni Bousera peridotite massif, North Morocco: derivation from subducted oceanic lithosphere. Earth Plan Sci Lett 102:289–301

Perry FV, Baldridge WS, Depaolo DJ (1987) Role of asthenosphere and kithosphere in the genesis of late Cenozoic basaltic rocks from the Rio Grande Rift and adjacent regions of the southwestern United States. J Geophys Res 92:9193–9213

Perry FV, Baldridge WS, Depaolo DJ (1988) Chemical and isotopic evidence for lithospheric thinning beneath the Rio Grande Rift. Nature 332:432–434

Porreca C (2005) Origin and modification of garnet pyroxenites in xenoliths from the Cerrito Negro, Rio Puerco volcanic field, New Mexico: a record of incipient lithospheric extension. MS thesis, University of New Mexico, Albuquerque p 139

Quade J, Cerling T, Bowman J (1989) Systematic variations in the carbon and oxygen isotopic composition of pedogenic carbonate along elevation transects in the southern Great Basin, United States. Geol Soc Amer Bull 101:464–475

Riter JCA, Smith D (1996) Xenolith constraints on the thermal history of the mantle below the Colorado Plateau. Geology 24:267–270

Roden MF, Irving AJ, Murthy VR (1988) Isotopic and trace element composition of the upper mantle beneath a young continental rift: results from Kilbourne Hole, New Mexico. Geochim Cosmochim Acta 52:461–473

Rosenbaum JM, Kyser TK, Walker D (1994a) High-temperature oxygen-isotope fractionation in the enstatite-$BaCO_3$ system. Geochim Cosmochim Acta 58:2653–2660

Rosenbaum JM, Walker D, Kyser TK (1994b) Oxygen isotope fractionation in the mantle. Geochim Cosmochim Acta 58:4767–4777

Rye D, Bradbury H (1988) Fluid flow in the crust: an example from a Pyrennean thrust ramp. Am J Sci 288:197–235

Ryerson FJ, McKeegan KD (1994) Determination of oxygen self-diffusion in akermanite, anorthite, diopside, and spinel—implications for oxygen isotopic anomalies and the thermal histories of Ca–Al-rich inclusions. Geochim Cosmochim Acta 58:3713–3734

Schulze D, Harte B, Valley J, Brenan J, Channer D (2003) Extreme crustal oxygen isotope signatures preserved in coesite in diamond. Nature 423:68–70

Sharp ZD (1990) A laser-based microanalytical method for the in situ determination of oxygen isotope ratios of silicates and oxides. Geochim Cosmochim Acta 54:1353–1357

Shaw CSJ, Thibault Y, Edgar AD, Lloyd FE (1998) Mechanisms of orthopyroxene dissolution in silica-undersaturated melts at 1 atmosphere and implications for the origin of silica-rich glass in mantle xenoliths. Contrib Mineral Petrol 132:354–370

Smith D (1987) Genesis of carbonate in pyrope from ultramafic diatremes on the Colorado Plateau, southwestern United States. Contrib Mineral Petrol 97:389–396

Smith D (1995) Chlorite-rich ultramafic reaction zones in Colorado Plateau xenoliths: recorders of sub-Moho hydration. Contrib Mineral Petrol 121:185–200

Smith D (2000) Insights into the evolution of the uppermost continental mantle from xenolith localities on and near the Colorado Plateau and regional comparisons. J Geophys Res 105:16769–16781

Smith D, Barron BR (1991) Pyroxene–Garnet equilibration during cooling in the mantle. Am Mineral 76:1950–1963

Smith D, Connelly JN, Manser K, Moser DE, Housh TB, McDowell FW, Mack LE (2004) Evolution of Navajo eclogites and hydration of the mantle wedge below the Colorado Plateau, southwestern United States. Geochem Geophys Geosys 5 DOI 10.1029/2003GC000675

Snyder GA, Taylor LA, Jerde EA, Clayton RN, Mayeda TK, Deines P, Rossman GR, Sobolev NV (1995) Archean mantle heterogeneity and the origin of diamondiferous eclogites, Siberia: evidence from stable isotopes and hydroxyl in garnet. Am Mineral 80:799–809

Staudigel H, Muehlenbachs K, Richardson S, Hart SR (1981) Agents of low temperature ocean crust alteration. Contrib Mineral Petrol 77:150–157

Taylor L, Snyder G, Keller R, Remley D, Anand M, Wiesli R, Valley J, Sobolev N (2003) Petrogenesis of group A eclogites and websterites: evidence from the Obnazhennaya kimberlite, Yakutia. Contrib Mineral Petrol 145:424–443

Ulmer P, Trommsdorff V (1995) Serpentine stability to mantle depths and subduction-related magmatism. Science 268:858–861

Usui T, Nakamura E, Kobayashi K, Maruyama S, Helmstaedt H (2003) Fate of the subducted Farallon plate inferred from eclogite xenoliths in the Colorado Plateau. Geology 31:589–592

Valley J, Kitchen N, Kohn M, Niendorf C, Spicuzza M (1995) UWG-2, a garnet standard for oxygen isotope ratios: strategies for high precision and accuracy with laser heating. Geochim Cosmochim Acta 59:5226–5231

van Achterbergh E, Griffin WL, Ryan C, O'Reilly SY, Pearsone N, Kivi K, Doyle B (2002) Subduction signature for quenched carbonatites from the deep lithosphere. Geology 30:743–746

Van der Lee S, Nolet G (1997) Seismic image of the subducted trailing fragments of the Farallon plate. Nature 386:266–269

Wang Y, McDonald E, Amundson R, McFadden L, Chadwick O (1996) An isotopic study of soils in chronological sequences of alluvial deposits, Providence Mountains, California. Geol Soc Amer Bull 108:379–391

Wawrzyniec T, Geissman J, Melker M, Hubbard M (2002) Dextral shear along the eastern margin of the Colorado Plateau: a kinematic link between Laramide contraction and Rio Grande rifting (ca. 75–13 Ma). J Geol 110:305–324

West M, Ni J, Baldridge WS, Wilson D, Aster R, Gao S, Grand S (2004) Crust and upper mantle shear wave structure of the southwest United States: implications for rifting and support for high elevation. J Geophys Res 109 DOI 10.1029/2003JB002575

Wilshire HG, Meyer CE, Nakata JK, Calk LC, Shervais JW, Nielson JE, Schwarzman EC (1988) Mafic and ultramafic xenoliths from volcanic rocks of the western United States. US Geol Surv Prof Paper 1443:179

Wilson D, Aster R, Ni J, Grand S, West M, Gao W, Baldridge WS, Semken S (2005a) Imaging the seismic structure of the crust and upper mantle beneath the Great Plains, Rio Grande Rift, and Colorado Plateau using receiver functions. J Geophys Res 110 DOI 10.1029–2004JB003492

Wilson D, Aster R, West M, Ni J, Grand S, Gao W, Baldridge WS, Semken S, Patel P (2005b) Lithospheric structure of the Rio Grande rift. Nature 433:851–855

Wyllie PJ, Lee WJ (1998) Model system controls on conditions for formation of magnesiocarbonatite and calciocarbonatite magmas from the mantle. J Petrol 39:1885

Xia Q-K, Dallai L, Deloule E (2004) Oxygen and hydrogen isotope heterogeneity of clinopyroxene megacrysts from Nushan volcano, SE China. Chem Geol 209:137–151

Yaxley GM, Green DH, Kamenetsky V (1998) Carbonatite metasomatism in the southeastern Australian lithosphere. J Petrol 39:1917–1930

Zhang HF, Menzies MA, Mattey DP, Hinton RW, Gurney JJ (2001) Petrology, mineralogy and geochemistry of oxide minerals in polymict xenoliths from the Bultfontein kimberlites, South Africa: implication for low bulk-rock oxygen isotopic ratios. Contrib Mineral Petrol 141:367–379

Zhang M, Suddaby P, O'Reilly S, Norman M, Qiu J (2000) Nature of the lithospheric mantle beneath the eastern part of the Central Asian fold belt: mantle xenolith evidence. Tectonophysics 328:131–156

Zhao Z-F, Zheng YF (2002) Calculation of oxygen isotope fractionation in magmatic rocks. Chem Geol 193:59–80

Zheng JP (1991) Calculation of oxygen isotope fractionation in metal oxides. Geochim Cosmochim Acta 55:2299–2307

Zheng JP (1993) Calculations of oxygen isotope fractionation in anhydrous silicate minerals. Geochim Cosmochim Acta 57:1079–1091